Accelerated Performance Degradation of Single-Phase Cold Plates for Direct-to-chip Liquid Cooled Data Centers

by

Lochan Sai Reddy Chinthaparthy

Presented to the Faculty of the Graduate School of

The University of Texas at Arlington in Partial Fulfillment

Of the Requirements

For the Degree of

MASTER OF SCIENCE IN MECHANICAL ENGINEERING

THE UNIVERSITY OF TEXAS AT ARLINGTON

DEC 2021

Supervising Committee:

Dr. Dereje Agonafer
Dr. Abdolhossein Haji-Sheikh
Dr. Rajesh Kasukurthy

UNIVERSITY OF TEXAS ARLINGTON

Acknowledgments

I would like to Thank Dr. Dereje Agonafer for the support and supervision he provided me throughout the time of my research in the EMNSPC Lab. I would also like to thank him for helping me with my thesis report and providing valuable tips for improving my work. I am particularly thankful to him for introducing me to various prospects to learn and recognize the practices used in the electronic cooling field.

I would like to thank Dr. A. Haji Sheikh and Dr. Rajesh Kasukurthy for providing me with their valuable guidance in improving my work and for serving on my dissertation committee.

I would like to thank Mr. Satyam Saini, Mr. Pratik Bansode, Mr. Pardeep Shahi, Mr. Vibin Simon Shalom, and Mr. Himanshu Modi for being my mentors and guiding me all over my time at EMNSPC Lab, and assisting me to put up this report.

Finally, I would like to thank my parents Mr. Chandrasekhara Reddy and Mrs. Sumana, and my friends for believing in me to achieve success in all my endeavors and for their unconditional love and support in every part of my life.

November 15, 2021

Abstract

Accelerated Performance Degradation of Single-Phase Cold Plates for Direct-to-chip Liquid Cooled Data Centers

Lochan Sai Reddy Chinthaparthy, M.S.

The University of Texas at Arlington, 2021

Supervising Professor: Dr. Dereje Agonafer

Expanding demands for cloud-based computing and storage, the Internet of Things, and AI-based applications have escalated thermal loads in high-density data centers which necessitated the utilization of more efficient cooling technologies. Direct-to-chip liquid cooling using cold plates has proven to be one of the most efficient methods to dissipate the high heat fluxes of modern high-power CPUs and GPUs. While the published literature has well-documented research on the thermal aspects of direct liquid cooling, a detailed account of reliability degradation is missing. The present investigation provides an in-depth analysis of the reliability degradation of copper cold plates used in high-power direct liquid cooling with accelerated failure conditions of flow rate and temperature. A benchtop setup is designed using a combination of different materials like Rubber tube copper cold plate, metal fittings, Instruments capable of measuring the thermal, hydraulic performance of the cold plate along with coolant chemistry (pH, ORP and Electrical Conductivity). The degradation was analyzed by time-based data for change in pH, ORP, and electrical conductivity as indicators of corrosion in the cooling loop. Non-destructive analysis of the cold plates was conducted change in channel dimensions using SEM, and microscopic analysis of the cold plate channels for copper pitting. These experimental results are presented in engineering design considerations for the construction of the flow loop and the choice of working liquid to be used.

List of Illustrations

List of Tables

List Of Graphs

Table of Contents

Introduction

Datacenter

A Datacenter in any organization is a facility that houses its critical applications and data. Its design is based on network, computing, and storage resources that enable the delivery of sharing applications and data. The core components of the data center are switches, routers, firewalls, storage systems, servers, and controllers. Artificial intelligence (AI) has become an important area that may significantly impact everyone’s daily life. This means a lot of high-performance chips such as high-performance CPU, GPU, FPGA (Field-programmable gate array), ASIC (application-specific integrated circuit) devices may need. The thermal design power (TDP) of these chips is high, and now it is very common to see a processor TDP reach as high as 300 watts.

Fig 1: liquid-cooled 1U rack data center[3]

The main component of the data center is the servers. Servers are classified based on their applications. Platform servers, Application servers, mail servers, proxy servers, web servers, and communication servers are a few of the types. The servers can be of different shapes and sizes according to their chassis design. The enclosure which holds the multiple servers is a rack. Rack-mounted servers are of standard sizes termed as 1U servers (1U=44 mm). This means if a server is a 2U size, it has a height of 2.5 inches.

Thermal Management of Datacenters

The equipment’s inside the Datacenters consumes a lot of power and thus dissipates a large amount. This requires the cooling of the equipment to operate at optimum temperature. As per a 2018 study on total energy consumption, it is observed that there is a total energy consumption of 205 terawatts of energy consumed by the data centers which is roughly 1% of energy consumption worldwide which is a total of 6% increase in energy consumption worldwide since 2010. These servers are required to operate at optimum temperature continuously without any interruption and thus cooling of servers inside the data center is important. Due to increasing environmental concern and increase in power consumption, the demand for more efficient cooling techniques has increased. There are three main types of data center cooling techniques

1. Air cooling
2. liquid cooling
3. immersion cooling.

The most traditional way and a common method of cooling data centers is Air cooling, but due to the increase in TDP at the chip level, the cooling efficiency by air cooling is not significant and thus in the modern world, the use of liquid cooling is suggested. For optimum cooling and designing purposes of these data centers American Society of Heating, Refrigerating and Air-Conditioning Engineers (ASHRAE) have created thermal guidelines for Liquid Cooling.

Classes	Typical Infrastructure Design		Facility Supply Water Temp (C)	IT Equipment Availability
	Main Cooling Equipment	Supplemental Cooling Equipment		
W1	Chiller/Cooling Tower	Water-side Economizer Chiller	2 – 17	Now available
W2			2 – 27	
W3	Cooling Tower	Chiller	2 – 32	Not generally available, dependent on future demand
W4	Water-side Economizer (with drycooler or cooling tower)	Nothing	2 – 45	
W5	Building Heating System	Cooling Tower	> 45	Specialized systems

Fig 2: 2011 ASHRAE Liquid-Cooled Thermal Guidelines

Liquid Cooling at Chip Level

In liquid cooling, a cold plate sits atop any heat-generating components such as CPUs, GPUs, etc. to extract the heat through single-phase cold plates. Generally, this type of arrangement has a higher heat removal capacity. This direct-to-chip level cooling can remove 70-75% of the heat generated by the equipment.

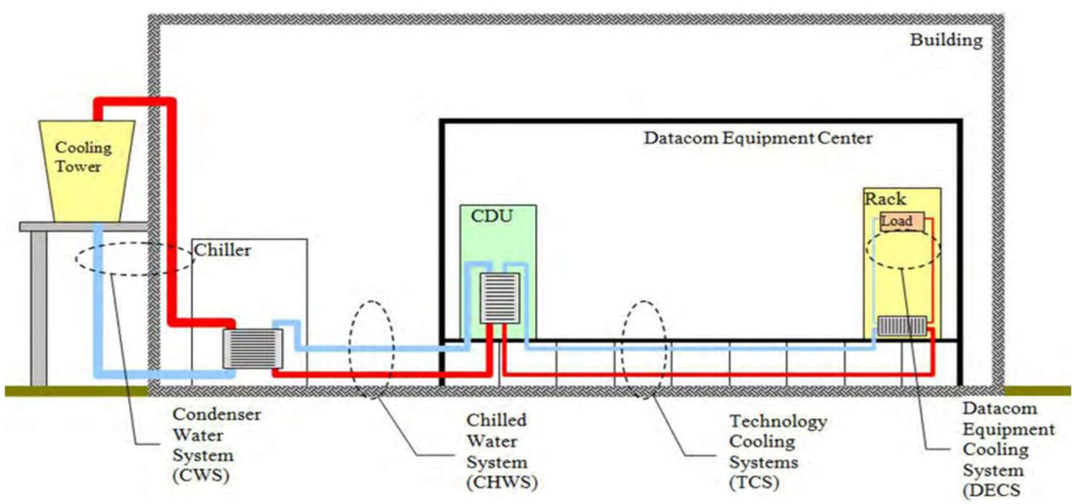

Fig 3: Schematic representation of Liquid Cooling facility

For single-phase liquid cooling, cold plates are looped with cooling fluid and the fluid is regulated via the use of Cooling Discharge Unit (CDU) to absorb heat from server components. The Cooling fluid is determined by balancing the thermal capture properties and the viscosity of the fluid in use. Water has the highest heat capture ratio but due to being less viscous it reduces the pumping efficiency and due to this it is often mixed with glycol, this decreases the heat capture capacity by increasing viscosity that enhances the pumping efficiency. Dielectric fluids can also be used but they generally have lower thermal transport capacity compared to water/glycol mixture.

Liquid Quality

The guidelines for the liquid quality are described in the Liquid Cooling Guidelines for Datacom Equipment Centers (ASHRAE 2014) to use the appropriate liquid at both the TCS and FWS level. The FWS system is often a site-wide or campus-wide building system, while the TCS loop is a data center-specific system and associated with a specific set of IT hardware. The TCS loop serves the IT equipment (ITE) and provides flow for cold plates and removing heat from electronic components. These cold plates and internal plumbing are far more sensitive to the liquid quality, as the liquid is in direct contact with the cold plate material, the material could get rusted and lead to impurities or resist the flow of the liquid, the potential issues are corrosion, fouling and microbial challenges.

Parameter	FWS (Table 5.3, ASHRAE 2014)	TCS (Table 6.2, ASHRAE 2014)
pH	7 to 9	8.0 to 9.5
Corrosion inhibitor(s)	Required	Required
Biocide	—	Required
Sulfide	<10 ppm	<1 ppm
Sulfate	<100 ppm	<10 ppm
Chloride	<50 ppm	<5 ppm
Bacteria	<1000 CFUs/mL	<100 CFUs/mL
Total hardness (as $CaCO_3$)	<200 ppm	<20 ppm
Conductivity	—	0.2 to 20 micromho/cm
Total suspended solids	—	<3 ppm
Residue after evaporation	<500 ppm	<50 ppm
Turbidity	<20 NTU (Nephelometric)	<20 NTU (Nephelometric)

Fig 4: Liquid Quality Guidelines by ASHRAE

Corrosion:

The disintegration of metal with its surrounding environment to form a chemically stable compound is called corrosion. It can also be called an electrochemical process in which oxides of the metal are formed in reaction with their surrounding media. The below-given equation is a general corrosion equation of any metal on reaction with water.

$$M + NH^{+} \rightarrow M^{N+} + 0.5NH_2$$

The below figure shows typical corroded copper metal when surrounded by any liquid media under corrosion suitable conditions.

Fig 5: corroded copper surface

Types of Corrosion: -

- Uniform corrosion
- Galvanic corrosion
- Crevice corrosion
- Pitting corrosion
- Selective corrosion
- Erosion corrosion
- Cavitation corrosion
- Flow assisted corrosion
- Stress corrosion

The two main corrosions which are seen on copper metal are Pitting and Galvanic corrosion.

Pitting Corrosion: -

It is localized corrosion that forms cavities on the metal surface which is initiated by oxidation of the surface. In the below fig we can see the formation of the pit on the surface.

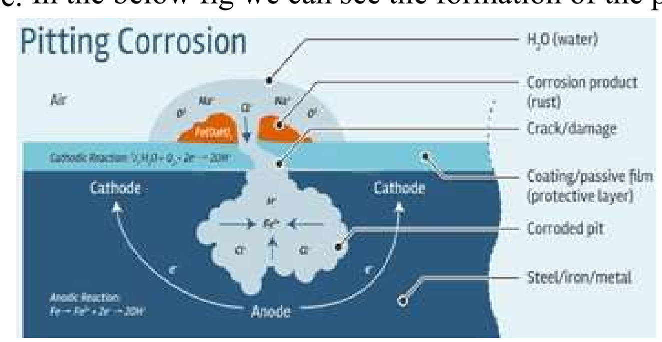

Fig 5.1: pitting corrosion[4]

Galvanic corrosion: -

This type of corrosion occurs between two dissimilar metals when immersed in the conductive solution and connected electrically. The cathode part is protected, and the anode part is corroded. In the below figure we can see the particles on the surface of the less noble part to be deposited on the more noble metal.

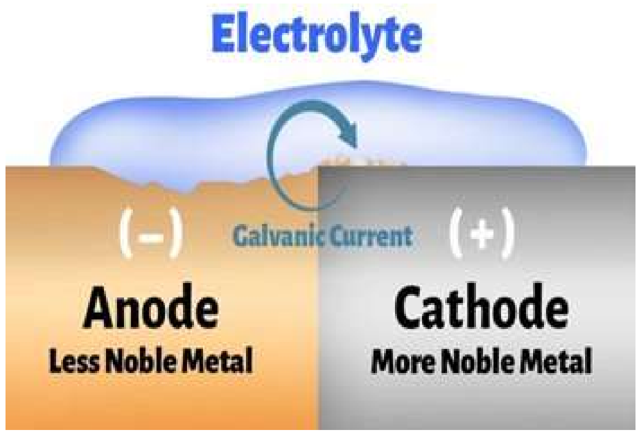

Fig 5.2: representation of Galvanic corrosion[5]

Effect of Corrosion

Corrosion in the loop can affect the functioning of a whole data center in multiple ways. When the copper metal gets corroded and copper oxide and copper hydroxide can be formed which are given in the below equations.

$$\mathrm{Cu}^{\circ} + \mathrm{H}_2^{\mathrm{I}}\mathrm{O} \longrightarrow \mathrm{Cu}^{\mathrm{II}}\mathrm{O} + \mathrm{H}_2^{\circ}$$

Fig 6.1: copper oxide formation reaction

$$\mathrm{Cu}^{2+} + 2\mathrm{H_2O} \rightarrow \mathrm{Cu(OH)_2} + 2\mathrm{H}^{+}$$

Fig 6.2: copper hydroxide formation reaction[1]

The formation of these compounds on the metal surface results in pores in the microchannel fin area which can disrupt the flow and higher pumping power might be needed to maintain the optimum flow condition another issue is the deposition of oxides can form blockages inside the channels and can result in leakages and failure of the whole loop which reduces the estimated life of the cold plate and increases the repair and maintenance cost.

Methods of detection

Corrosion in the loop can be detected either in the variation of chemical properties like pH, electrical conductivity, and oxidation-reduction potential of coolant liquid or by observing the variation of performance of the cold plate-like thermal resistivity and pressure difference.

pH

pH is a value that defines the acidity of the liquid. It is a measure of the concentration of hydrogen ions in any liquid. Its value ranges from 0- 14.

$$pH = -\log_{10}(H^+)$$

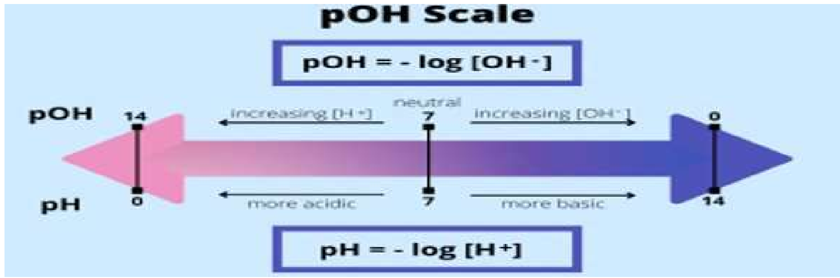

Fig 7.1: pH scale

Electrical Conductivity (EC)

It is a measure of the concentration of charged particles in the respective liquid that move around freely. Conductivity is itself carried ions in the liquid, more the ions the conductivity. Its units are ‘siemens’.

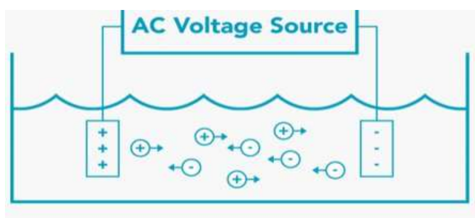

Fig 7.2: travel path of charged ions in a liquid[7]

Oxidation-reduction potential:

ORP is a measurement of the liquid that defines the ability of the liquid to either oxidize or reduce other substances. Its units are in ‘mV’. The higher the ORP value the higher the ability of the liquid’s oxidizing capability.

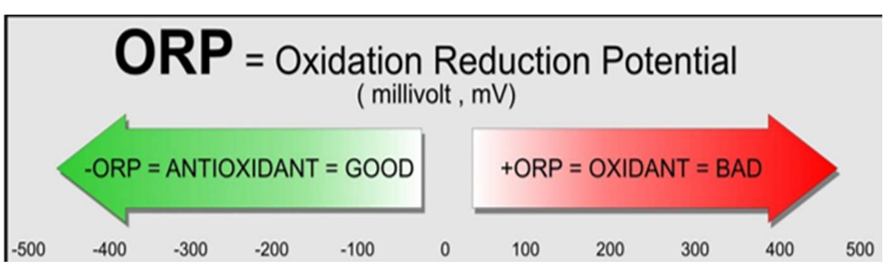

Fig 7.3: General ORP scale[6]

Thermal resistance:

It's the ratio of the temperature difference between the base of the heat source and the inlet coolant temperature to the power supplier to the heat source. With the increase of corrosion in the cold plate the thermal resistance decreases.

$$\Psi j,in=(Tj-Tin)/Power$$

Pressure difference:

The difference between inlet and outlet pressure across the cold plate. It can be represented as 'ΔP'.

$$\Delta P=Pin-Pout$$

Objective

Under general conditions, any copper metal doesn't corrode on reaction with water, unless there is any chemical mixture in the liquid or the liquid flowing on the metal surface is at an elevated temperature. The main objective of this research is

- To determine the change in pH Electrical conductivity and ORP values of the coolant liquids.
- To observe the variation of performance of the cold plate.
- To compare the variation of coolant chemical properties under the stagnated condition at elevated temperatures with a combination of different metallic compounds immersed in it.

List of liquid coolants

Name	Composition	properties
Inhibited PG-55	55%PG+45% water+ corrosion Inhibitors	Freezing point -43.3 °C Boiling point -106.1 °C Density – 1.042g/ cm^3 Viscosity – 6.19mPa.s Thermal conductivity- 1.5615W/m^2·K colorless
Inhibited PG-25	25%PG+75% water + corrosion Inhibitors	Freezing point -10.1 °C Boiling point -101 °C Density – 1.021g/ cm^3 Viscosity – 2.45mPa.s Thermal conductivity - 1.1357W/m^2·K colorless
Inhibited EG-25	25%EG+75% water + corrosion Inhibitors	Freezing point -12.6 °C Boiling point -103.1 °C Density – 1.040g/ cm^3 Viscosity – 2.09mPa.s Thermal conductivity - 1.582W/m^2·K colorless
Inhibited EG-55	55%EG+45% water + corrosion Inhibitors	Freezing point -45.3 °C Boiling point -107.9 °C Density – 1.088g/ cm^3 Viscosity – 5.77mPa.s Thermal conductivity - 1.215W/m^2·K colorless

Literature Review

In recent studies, experiments were conducted to elucidate down select the wetted materials and components which are best suitable for the loop. The experiments were kept running for more than 600 hours. The thermal performance and coolant properties were monitored during the experiment period. After analyzing the data from these experiments, it was seen that the degradation of the cold plate was increasing with an increase in temperature. The changes in the coolant properties like pH, electrical conductivity also proved the progression of corrosion. A soak test of the wetted materials was performed and the depletion of charged particles with time was observed the conductivity of the liquid was varying with the initial condition.[1]

Experiments were carried out to investigate the corrosion mechanism caused by galvanic corrosion across the brazed alloy present in the cold plate microchannels. The investigation proves that the galvanic potential between the brazed plate and copper are the main factors for a higher corrosion rate in the loop. An effective kinematic model consisting of factors like temperature and external voltage was proposed to predict the reliability failure of engineering components. These factors act as accelerators to increase the corrosion rate. The results have shown an increase in galvanic potential over time across the test piece which can be a threat to the corrosion reliability of the cold plate. Through the images of surface topography obtained from the Scanning electron Microscope, the damages on the surface were observed by corrosion reaction.[2]

Chapter 3

Experimental Setup and Procedure

Methodology

Corrosion is an electrochemical process that can be detected either on the surface or in the media surrounding the surface. The media used in the experiment is coolant liquids which are used in real-time data center cooling applications. The change of the coolant chemistry can be detected by logging the pH, electrical conductivity, and Oxidation Reduction Potential (ORP) values from time to time.[21]

On the surface, which is the cold plate microchannel area, the corrosion can be detected by two methods. The first method is to observe the surface topography and composition by using a device called the scanning electron microscope (SEM) which can give, and the other method is by comparing the values of the Thermal resistance and pressure drop across the cold plate from time to time.[22]

A single bench-top setup shown in Fig is built to monitor pH, EC, ORP values of the liquid in the reservoir. The outlet and inlet temperature values of the cold plate are noted to observe the pressure difference and thermal resistance during the duration of the experiment for each of the liquids used individually.[23]

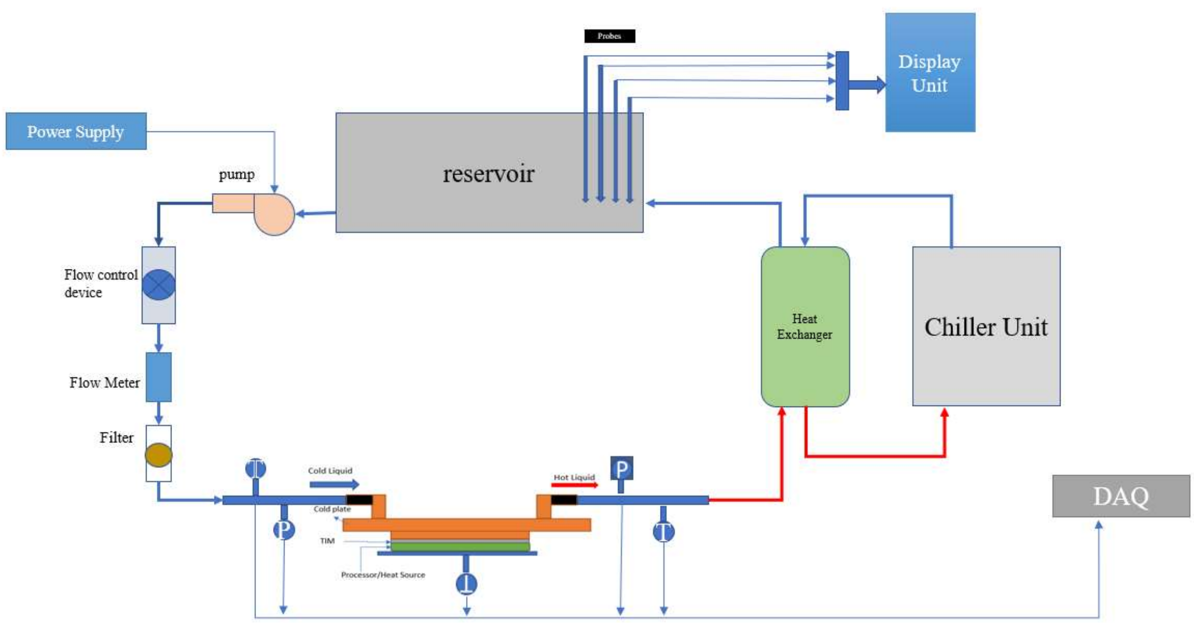

Fig 8: Schematic representation of the Benchtop Setup

Experimental Setup – I

This experiment is a closed-loop single benchtop setup. A Fluid Reservoir made of BPA-free plastic is used to avoid any chemical reaction with liquid coolant. A 12V DC centrifugal pump is attached to the reservoir to pump the fluid into the cold plate. A precision flow control device is used to maintain the required flow rate which can be observed using a flow meter. Thermistor and Pressure sensors are connected before and after the cold plate to measure inlet and outlet values of temperature and pressure of the flow. Cold Plate consisting of microchannels is attached to a ceramic heater of 1000Watt capacity with thermal interface material to achieve maximum heat transfer. A Micromesh filter is introduced into the loop to remove any unwanted dust particles present in the liquid coolant. A heat exchanger unit is attached right before the reservoir to maintain coolant liquid at the desired temperature. pH, EC, ORP, Temperature sensing probes are kept in the reservoir and connected to the display unit. Pressure sensors are connected to a DC power supply unit along with the centrifugal motor. A K-type thermocouple is kept in between a ceramic heater and a cold plate to measure the base temperature when power is given through a 120V DC power supply. All the thermistors, pressure sensors, thermocouples, and Probes are connected to a Data Acquisition Unit for data logging.[24]

List of equipment

Name	Image	Properties
Microchannel cold plate	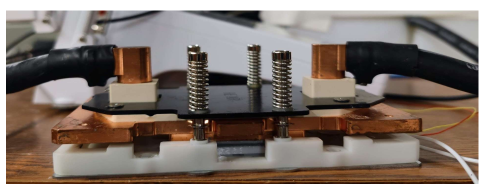 Fig 9: cold plate	Material - Copper
Ceramic Heater	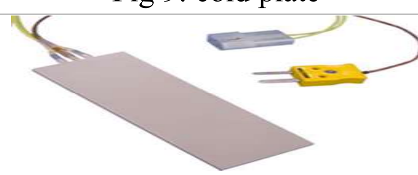 Fig 10: Ceramic Heater[8]	Material - Aluminum Nitride Max temperature – 400°C Max Power – 1000 Watt
Centrifugal pump	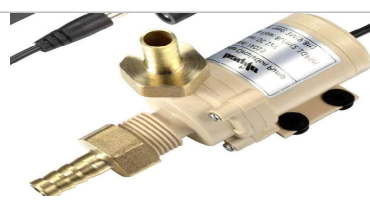 Fig 11: Centrifugal pump[9]	Power source – 12V DC Max Flow rate – 8lpm Max Head – 3m Material – plastic

Flowmeter	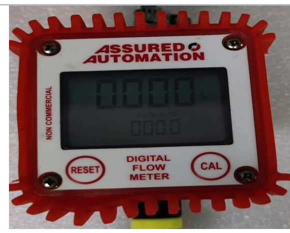 Fig 12: flowmeter	Flow rate – 0.083lpm to 5 lpm Temp range - -40°C to 80°C Max pressure - 145psi Accuracy - +/- 1% Material – Pa66 + GF/PPs
Thermistor 10K sensor	 Fig 13: thermistor	Material – Brass
Pressure Sensor GP-M001	 Fig 14: pressure sensor[10]	Range - -14.5 to 145 PSI Medium temperature - -20 to +100°C Power voltage – 10-30V DC Material - SS304
Flow control valve	 Fig 15: flow control valve[11]	Material – 316SS Max Pressure – 200PSI Temperature range - -17.5 to 176°C
Micromesh	 Fig 16: Microfilter[12]	50µm Mesh(SS) Material Housing – polypropylene Bowl material - Nylon
Brazed plate heat exchanger	 Fig 17: heat exchanger[15]	Max pressure 580psi Max temperature 200°C Material Copper and Nickel
PolyScience Chiller	 Fig 18: Chiller unit[13]	Max power – 10KW Operating range – 10 to 50°C Max pressure – 100PSI Max Flow – 13.2lpm

Power supply E3642A	 Fig 19: power supply unit	Output range – 30 to 100W Low range 0 to 30V/2.2A High range 0 to 60V /1.3A
Agilent DAQ Unit	 Fig 20: DAQ unit	2-wired 22 channel inputs 20 voltage inputs Two current inputs
Reservoir	 Fig 21: insulated reservoir	Polypropylene Capacity - 3Gallons
HI5522	 Fig 22: HI5522 Display unit[15]	12V DC power supply pH range - -2 to 20 EC range – 0US to1000mS Temperature range - -20 to 120°C ORP range - =/- 2000mv
HI1131B	 Fig 23: pH sensor[16]	Material - Glass Reference Ag/AgCl Electrolyte 3.5M KCL Temperature range – 0 to 100°C
HI76312	 Fig 24: conductivity sensor[17]	Platinum electrode Range 0 to 1000mS Temperature range - -5 to 100°C
HI3131B	 Fig 25: ORP sensor[18]	Material - glass Temperature range - -5 to 70°C Tip platinum pin

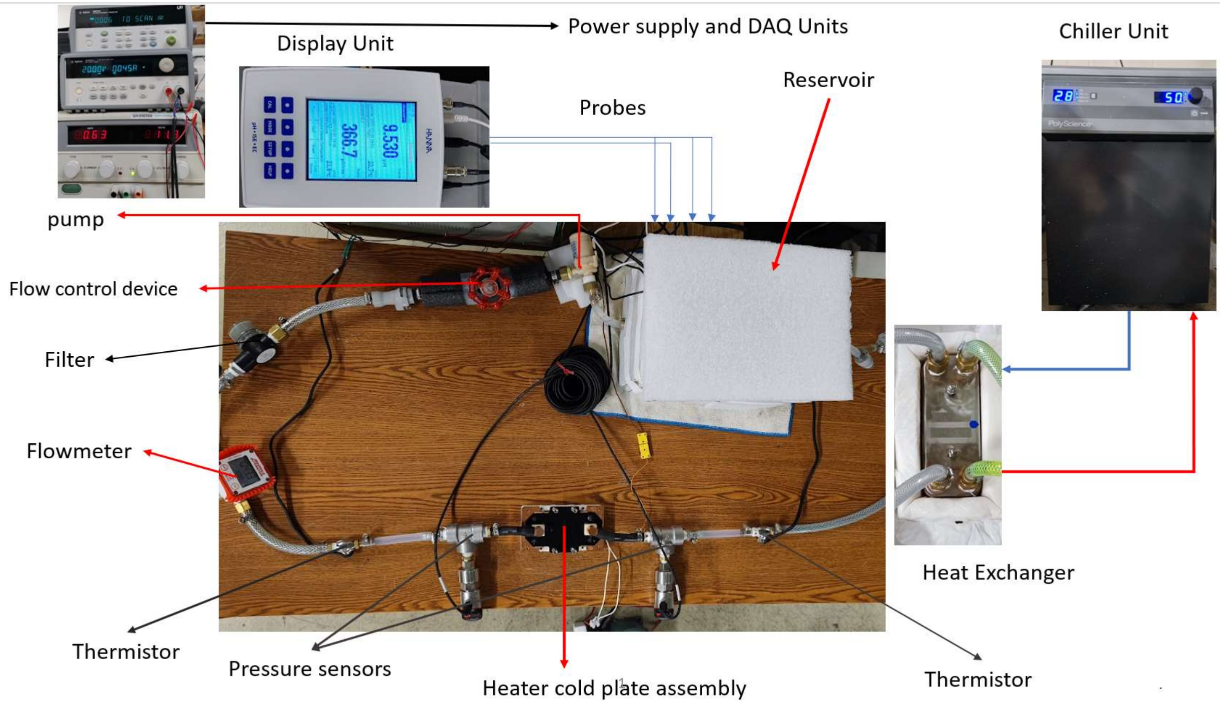

Fig 26: final image of Benchtop setup

Experiment – I Procedure

1. Pour DI water into the Loop and run the pump for a little while.
2. Add 10ml of Spectrus NX100 solution into the DI water and keep the loop running for a few more minutes which can remove any salts or any other precipitates from all the surfaces through which coolant liquid flows.
3. Remove the Di water and Spectrus NX100 solution and add fresh Di Water again into the Loop.
4. Run the Loop again for a few minutes and remove the Di water. This step is performed to remove and left-over residues in the loop.
5. Add the desired quantity of Coolant Liquid in the loop and switch ON the pump.
6. After all the air from the loop is removed add a few more amounts of liquid if required.
7. Keep the pump at max power to ensure all the air bubbles are removed in the loop.
8. Insert the pH, EC, ORP, Temperature sensing probes into the reservoir and make sure there is sufficient liquid in the reservoir such that an ample amount of liquid is in contact with the probes.[25]
9. Power up the ceramic Heater to 350watts.
10. Adjust the flow rate to 0.5 lpm using the flow control device and switch ON the Chiller Unit keeping the temperature at 50°C.
11. The reservoir inlet coolant liquid will be approx. 50°C as the remaining heat is reduced in the heat exchanger.

12. After the loop reaches stable condition start the DAQ unit so that all the thermistors, pressure sensors, thermocouple, and Probes values are stored in the local PC.
13. Note down the average values of each entity for every hour.
14. The values of pH, EC, and ORP at that instant of each hour should be noted and plotted on a graph.

Experiment – II Setup

The second experiment is conducted to observe the change of coolant chemistry concerning the time at elevated temperatures when kept in stagnated conditions. Two sets of four jars are kept in an environmental chamber shown in fig. The first set is kept unopened through the experiment and the other set of jars are opened twice every 24 hours and are exposed to the outside air. The idea of exposure to outside air refers to the amount of time coolant liquids in a data center are exposed during maintenance filter change and other operations. This time is approximately around 1 to 3% of the time for which a liquid is used.

There are two variations in this experiment. In the first variation, the liquids are kept without any addition of suspended materials and the readings are observed for 240 hours. In the second variation combination of different materials like copper, Stainless Steel, Brass, and EPDM rubber is kept immersed in all eight jars. This variation is to see the effect on coolant chemistry with the presence of different combinations of materials. [26]

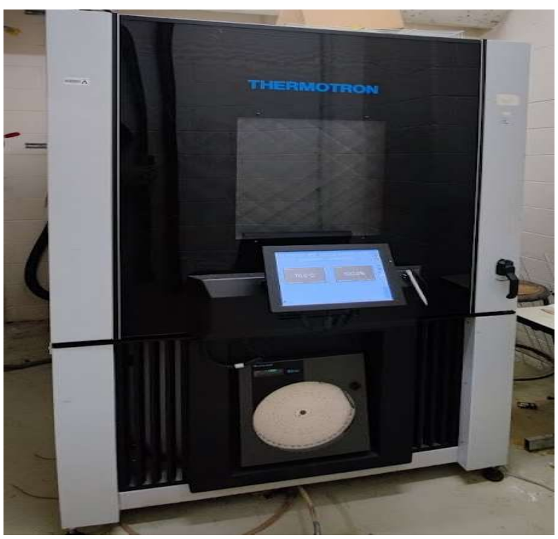

Fig 27: Environmental chamber


Fig 28: Borosilicate jars[19]

Experiment – II Procedure

Variation – I

1. In the first variation test two sets of jars are prepared, each set containing four jars for four different liquids.
2. Clean all the Borosilicate jars with DI water twice.
3. Rinse the jars with their allocated liquid and fill the jar with ¾ quantity of liquid.
4. Set-I jars are kept closed at elevated temperature for the entire time and the initial and final values of pH, EC, ORP, Temperature are noted.
5. The other set of jars which is also kept at the same elevated temperature is exposed to atmospheric air for approximately 3%
6. of the entire time and their pH, EC, ORP, Temperature values are noted twice a day.
7. Place the jars inside the environmental chamber and edit the program.
8. Keep the temperature inside the chamber at 70°C and 40% humidity.
9. Save the program and run it.[27]

Fig 29: Variation – I jars kept in Environmental chamber

Variation – II

1. In the second variation test two sets of jars are prepared, each set containing four jars for four different liquids.
2. Clean all the Borosilicate jars with DI water twice.
3. Rinse the jars with their allocated liquid and fill the jar with ¾ quantity of liquid.
4. Place different materials such as LPDM rubber tubes, copper plates, bars of brass, and stainless steel each of one quantity inside the jars after removing all the impurities on them.

Fig 30: different metals immersed in the liquid

5. Set-I jars are kept closed at elevated temperature for the entire time and the initial and final values of pH, EC, ORP, Temperature are noted.
6. The other set of jars that are also kept at the same elevated temperature is exposed to atmospheric air for approximately 10% of the entire time and their pH, EC, ORP, Temperature values are noted twice a day.
7. Place the jars inside the environmental chamber and run the same program as in variation – I.

Fig 31: Variation – II jars kept in Environmental chamber

Calibration:

Thermistor calibration

The calibration of the thermistor is done by the Thermistor calibration bath shown in the figure below. The thermistors are kept immersed in the thermal bath. A program is set from 15 to 80 and is kept running till the temperature of the liquid inside the bath reaches both the given setpoints. The thermistor reading is noted at both setpoints. Offset and gain values are calculated and are fed to the DAQ unit.[28]

Fig 32: Thermistor calibration bath[20]

Pressure sensor calibration

The calibration of the pressure sensors is done by the Pneumatic Pressure Comparator P5510 shown in the figure below. the sensor is attached at another end of the air outlet. The knob is pressed down after closing the exhaust valve. Multiple readings are noted and the mean of difference in the values is calculated and is fed to the DAQ unit. Offset and gain values are calculated and are fed to the DAQ unit.

Fig 33: Pneumatic Pressure Comparator P5510

Flowmeter calibration

Coriolis flowmeter fig is a device that shows the accurate flow rate of a liquid irrespective of the viscosity of the liquid. The digital flow meter is connected in series with the Coriolis flowmeter and a pump is connected to give a flow in the loop. The flow rate is varied and the readings of both the flow meters are noted, after calculating the offset value it is adjusted in the digital flow meter.

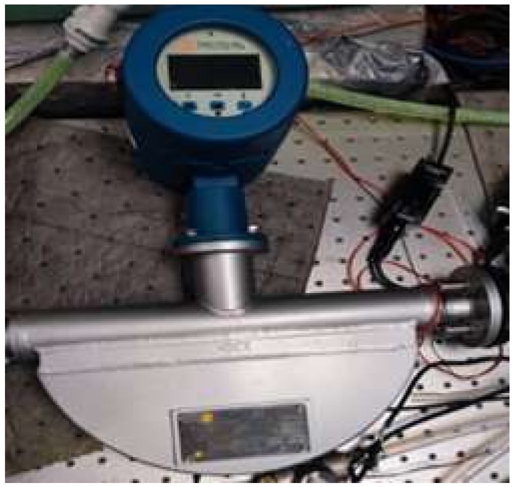

Fig 34: Coriolis Mass Flow Meter

pH and Conductivity sensor calibration

The display unit HI5522 is set on calibration mode. The pH electrode along with the temperature sensing probe is inserted in 4 different liquids which have some standard pH values at certain temperatures. The probe sends the values to the display unit and calibrates them automatically. In a similar way the conductivity sensing probe is set at calibration mode and the sensor is kept immersed in a liquid with a standard EC value. The display unit automatically calibrates the probe. In the below Fig and Fig, we can see four different liquids in which pH and Temperature probes are kept inserted and the conductivity probe is kept immersed.

Fig 35: calibrating liquids with standard pH values Fig 36: Standard conductivity solution

Results

Experiment – I

EG-25

The benchtop setup is used to experiment on EG-25 coolant liquid. The values are logged into a computer through a data acquisition unit. The result of the logged values for the EG-25 are plotted on the graphs below.

On corrosion reaction oxides of copper are formed which are stable and have less thermal resistivity than pure copper. From the increase in thermal resistivity as shown in the graph in the duration of the experiment we can say that the surface of the microchannel cold plate is corroded which can affect the life of the cold plate.[29]

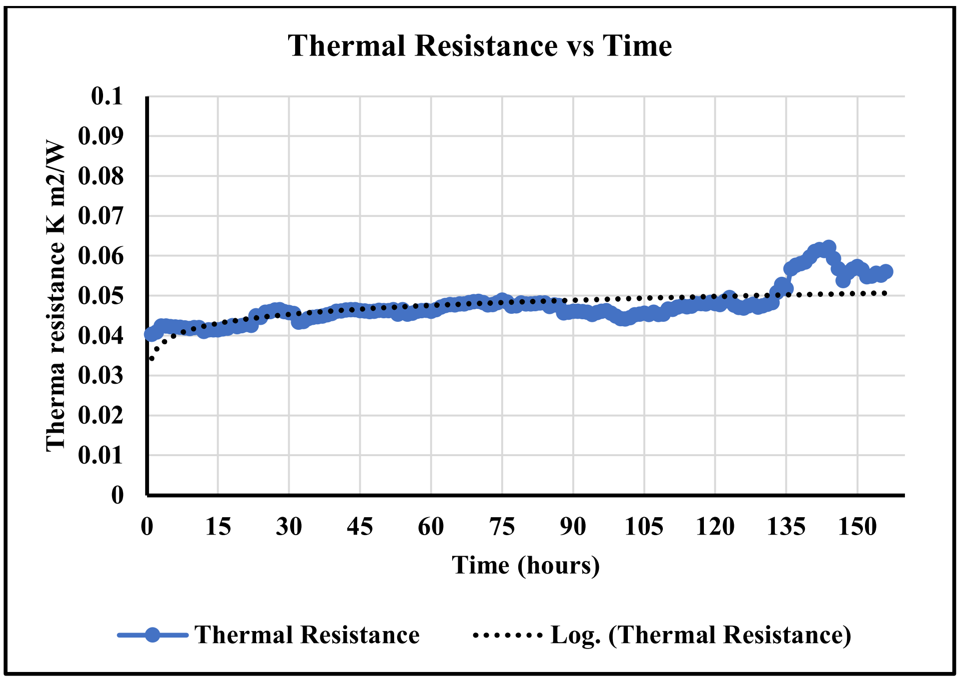

Graph 4.1.1: Thermal resistance vs Time of EG-25

From the graph, we can say that due to the corrosion reaction pores and cavities are formed inside the cold plate microchannel area which results in disrupting the flow of coolant across the cold plate and results in an increase of pressure drop across it. The sudden increase of pressure difference around 110 hours is due to elevating the rear end of the reservoir to increase the head level of liquid inside the reservoir as the liquid level was decreasing because of evaporation.[30]

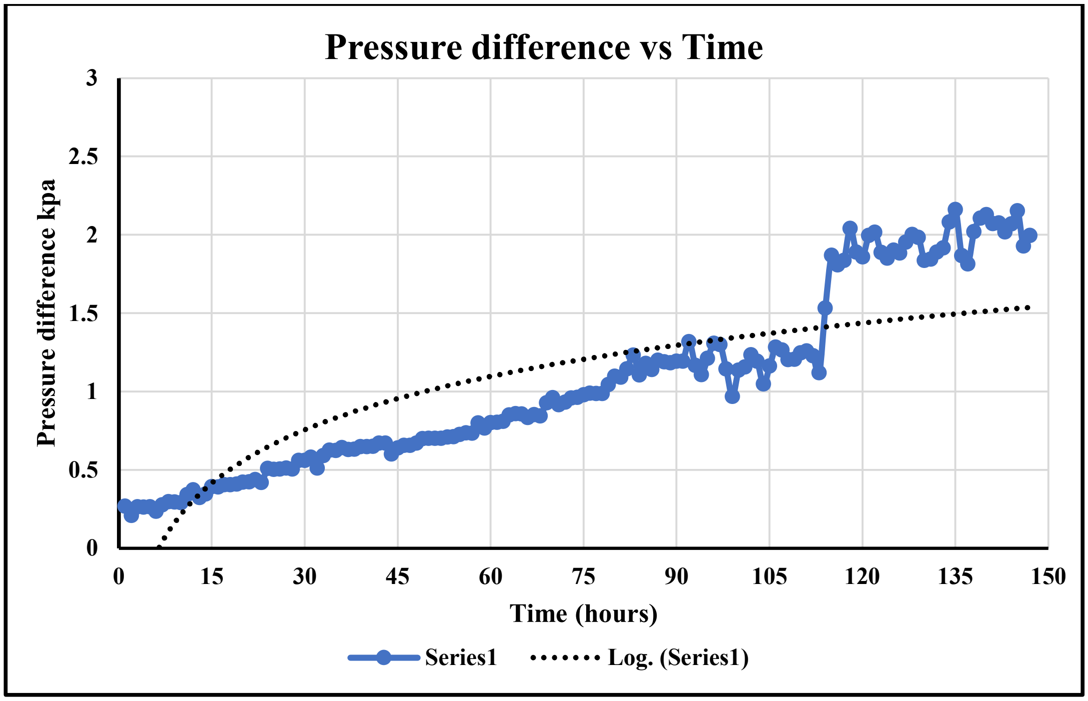

Graph 4.1.2: Pressure difference vs Time of EG-25

The pH value is seen to decrease over time in the graph. This is due to an increase in H+ ion concentration in the liquid which is released with the formation of copper oxides. Initially, during the first 40 hours, the value pH is decreased at a higher rate due to the initial passivation reaction. Later, the pH value is almost stable throughout the experiment.[31]

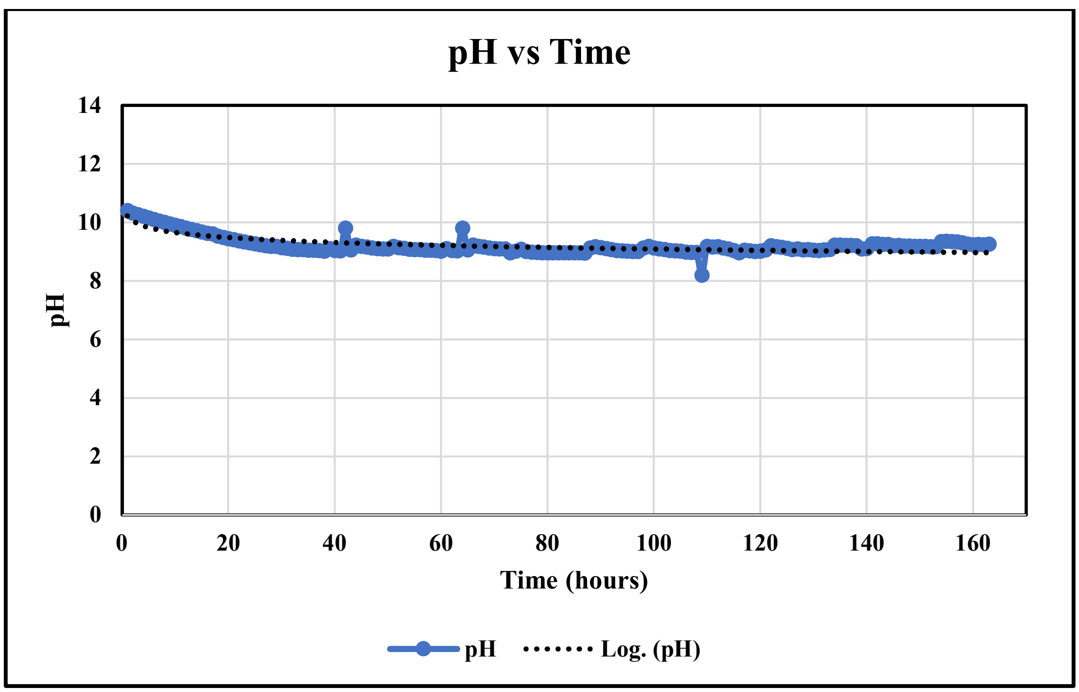

Graph 4.1.3: pH vs Time of EG-25

The conductivity of the liquid at different intervals of time is observed in the graph below the conductivity value reduces due to the loss of charge carriers in the liquid which reduces the rate of corrosion. These charge carriers are initially added as corrosion inhibitors which deplete as time passes by. The fluctuation of the graph observed is due to the exposure of outside air to the reservoir for the removal of probes during their calibration process.[32]

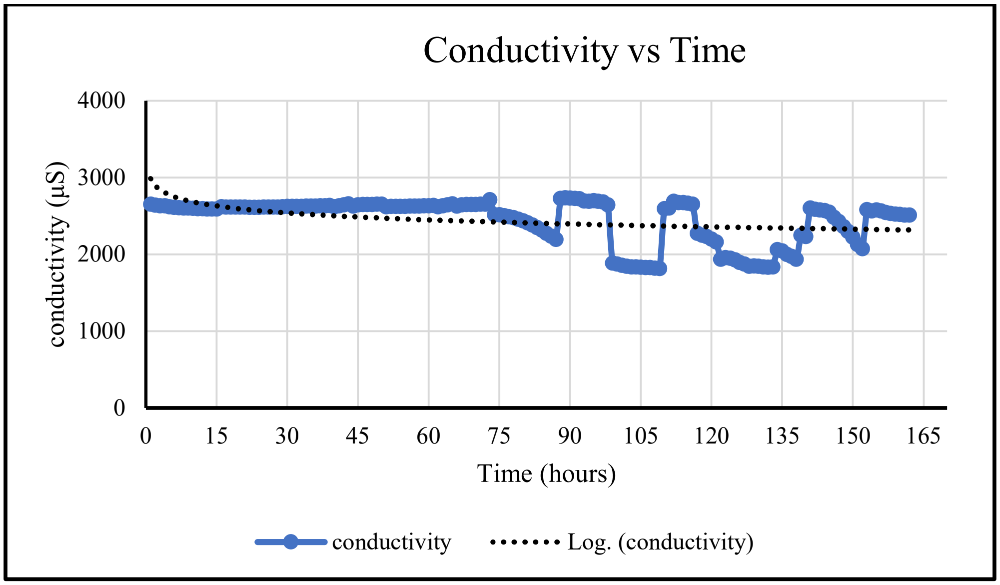

Graph 4.1.4: Electrical Conductivity vs Time of EG-25

The ORP represents the oxygen levels in a liquid. In the below graph the ORP of EG-25 is seen to be increasing concerning time which tends that the oxygen level in the liquid is increasing which can result in a higher corrosion rate in the loop.

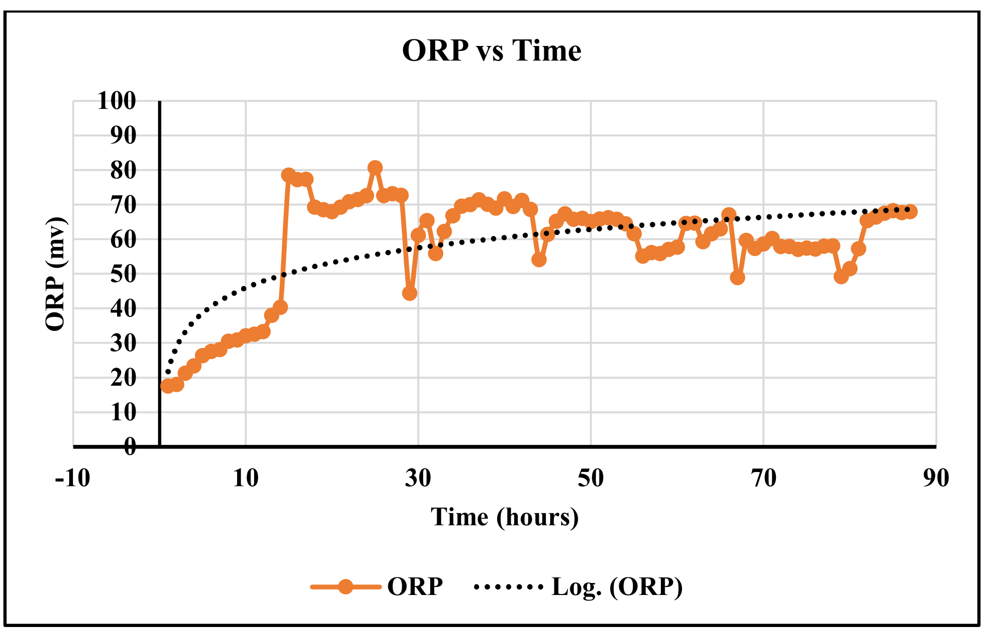

Graph 4.1.5: ORP vs Time of EG-25

PG-55

The benchtop setup is used to experiment on PG-55 coolant liquid. The values are logged into a computer through a data acquisition unit. The result of the logged values for the PG-55 are plotted on the graphs below.

On corrosion reaction oxides of copper are formed which are stable and have less thermal resistivity than pure copper. From the increase in thermal resistivity as shown in the graph in the duration of the experiment we can say that the surface of the microchannel cold plate is corroded which can affect the life of the cold plate.[33]

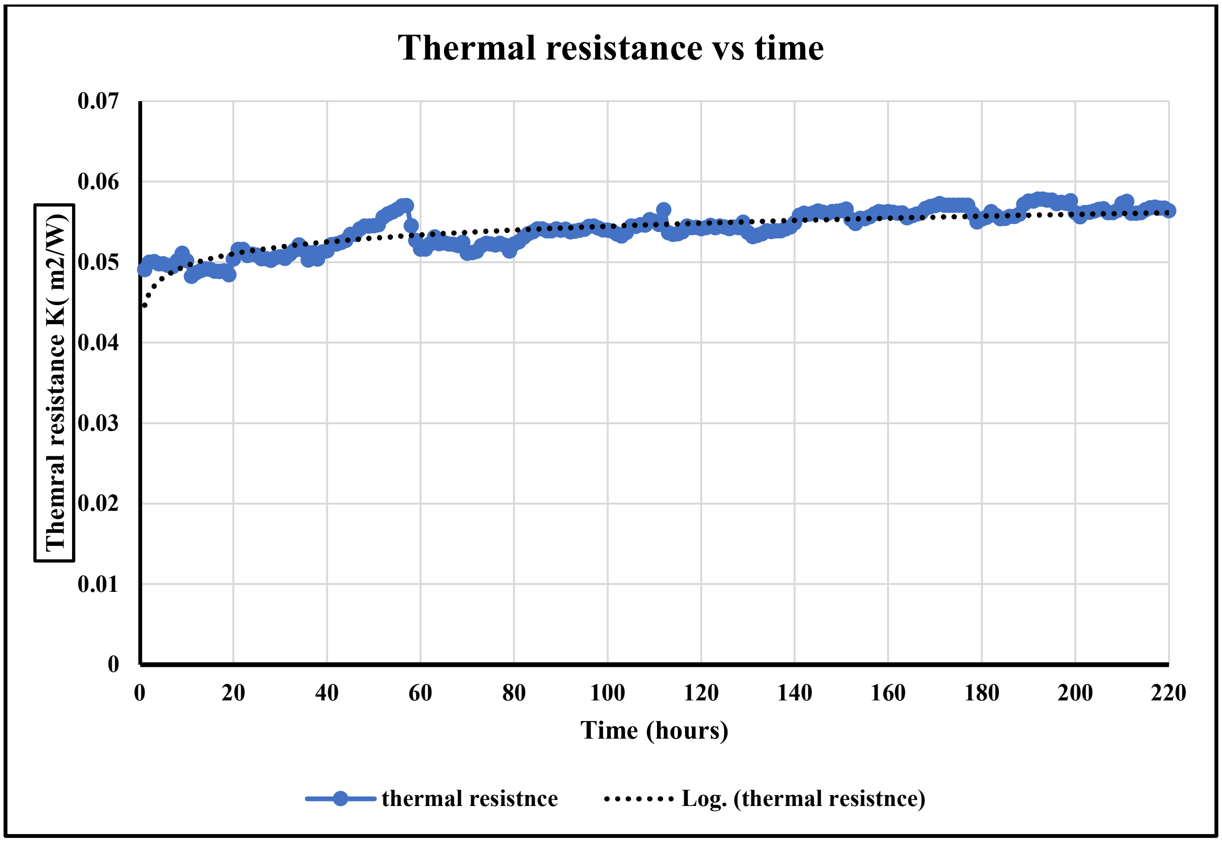

Graph 4.2.1: Thermal resistance vs Time of PG-55

From the graph, we can say that due to the corrosion reaction pores and cavities are formed inside the cold plate microchannel area which results in disrupting the flow of coolant across the cold plate and results in an increase of pressure drop across it. The trendline of the Graph indicates the mean pressure increase throughout the experiment.

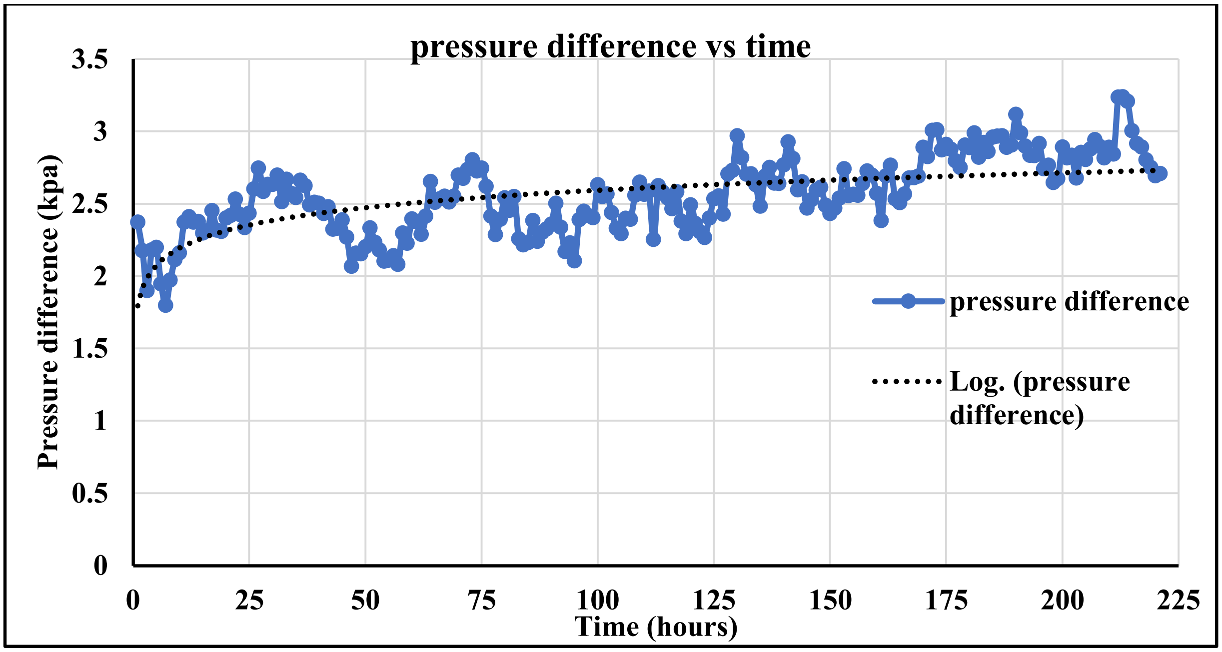

Graph 4.2.2: Pressure difference vs Time of PG-55

The pH value is seen to decrease over time in the graph. This is due to an increase in H+ ion concentration in the liquid which is released with the formation of copper oxides. Initially, during the first 40 hours, the value pH is decreased at a higher rate due to the initial passivation reaction. Later, the pH value is almost stable throughout the experiment.

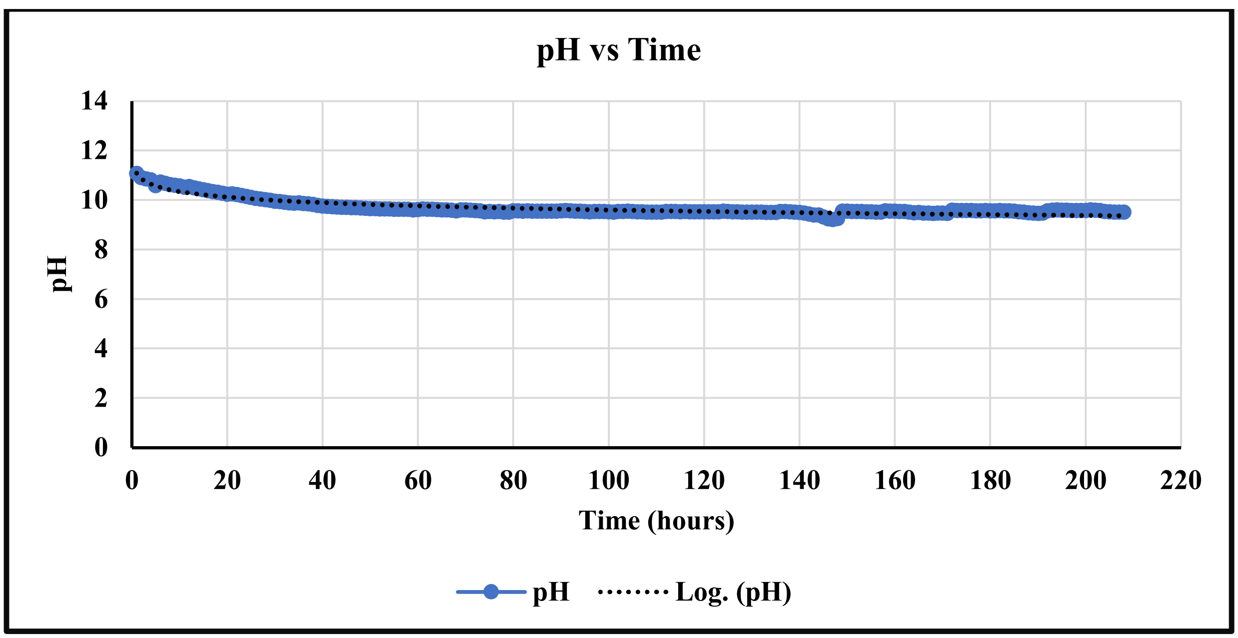

Graph 4.2.3: pH vs Time of PG-55

The conductivity of the liquid reduces due to the loss of charge carriers in the liquid which reduces the rate of corrosion. These charge carriers are initially added as corrosion inhibitors which deplete as time passes by. The charge carriers supply charged ions to the copper surface to nullify the imbalance and prevent the formation of copper oxides. [34]

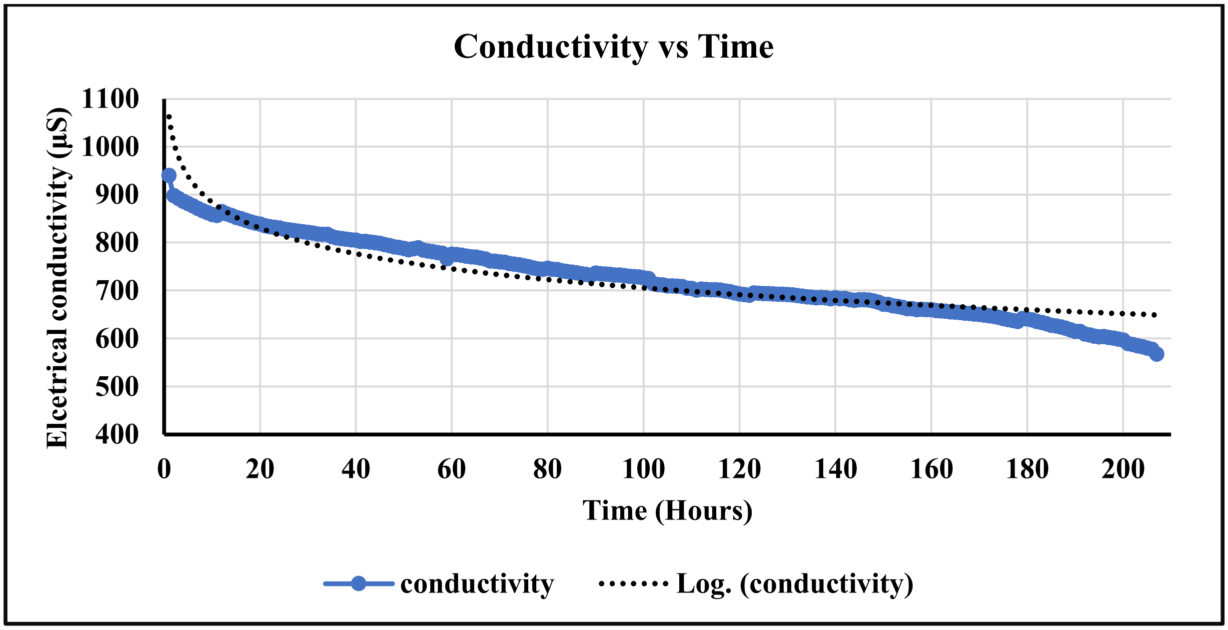

Graph 4.2.4: Electrical Conductivity vs Time of PG-55

The ORP value of PG-55 is seen to be increasing over time which tends that the oxygen level in the liquid is increasing which can result in a higher corrosion rate in the loop. The fluctuation of ORP is due to the exposure of liquid to outside air during the removal of sensing probes for calibration purposes.

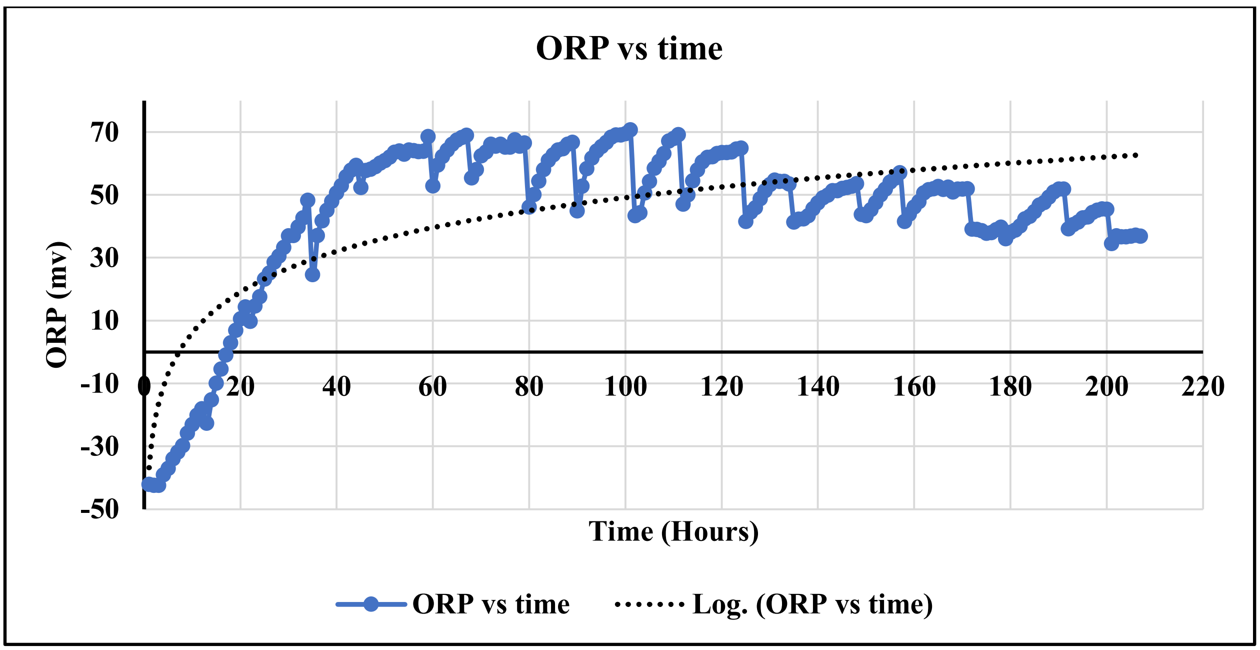

Graph 4.2.5: ORP vs Time of PG-55

Experiment – II

Variation – 1

Set – I (pH)

The pH values of all the liquids are measured initially and compared to the pH value at the end of the experiment. The set-1 jar is unexposed to outside air during the whole test. From the below graph we can say that all the liquids have a similar trend in pH levels. EG-55 has a 3.9% change which is the least while EG-25 has a 5.07% change as the highest change among the four liquids in pH value.

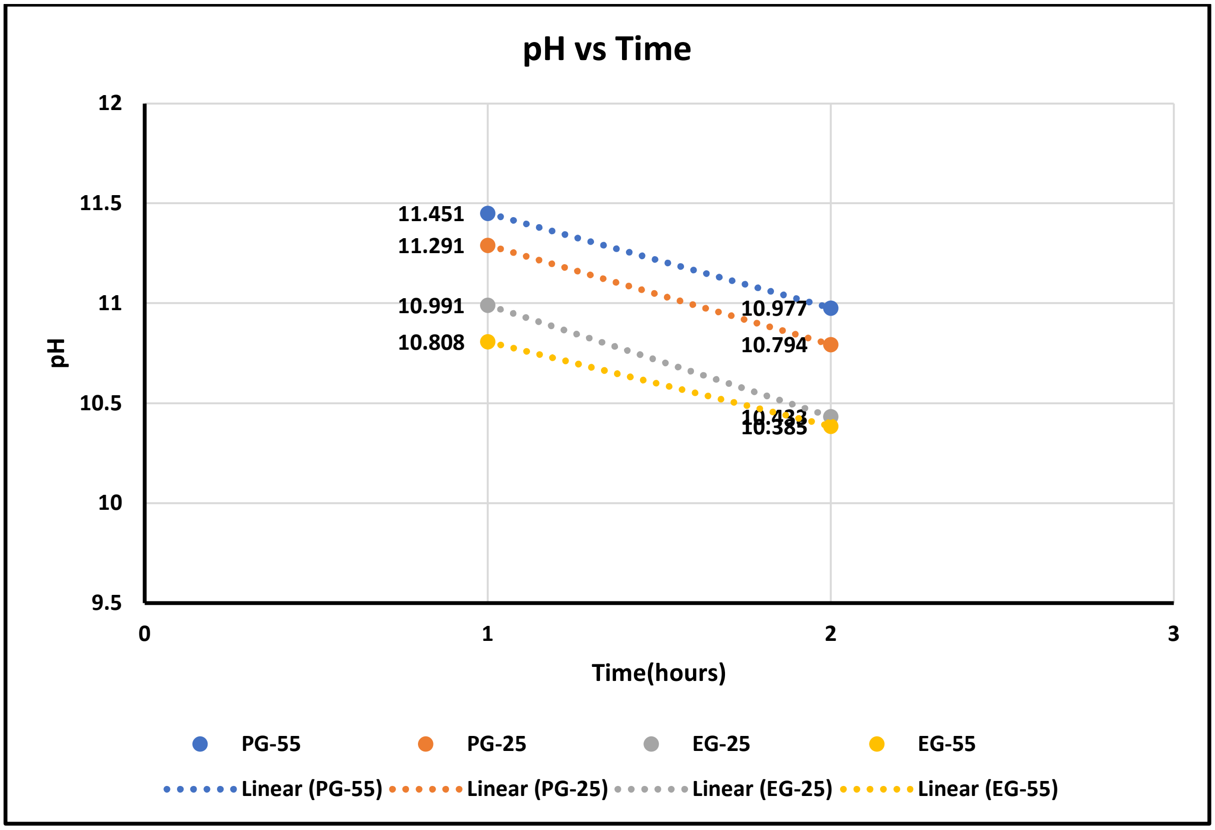

Graph 4.3.1.1: Variation – I Set – I pH vs Time

Set – II (pH)

In the second set of jars which were exposed to the outside air for a period approximately 1-2% of the time, the readings were taken twice every day with 12 hours gap. From the below graph it is observed that all the liquids have a similar trend in pH levels even with periodic exposure to the outside air. PG-55 has the least change of 8.87% and PG-25 has the highest change of 10.3% in pH value.

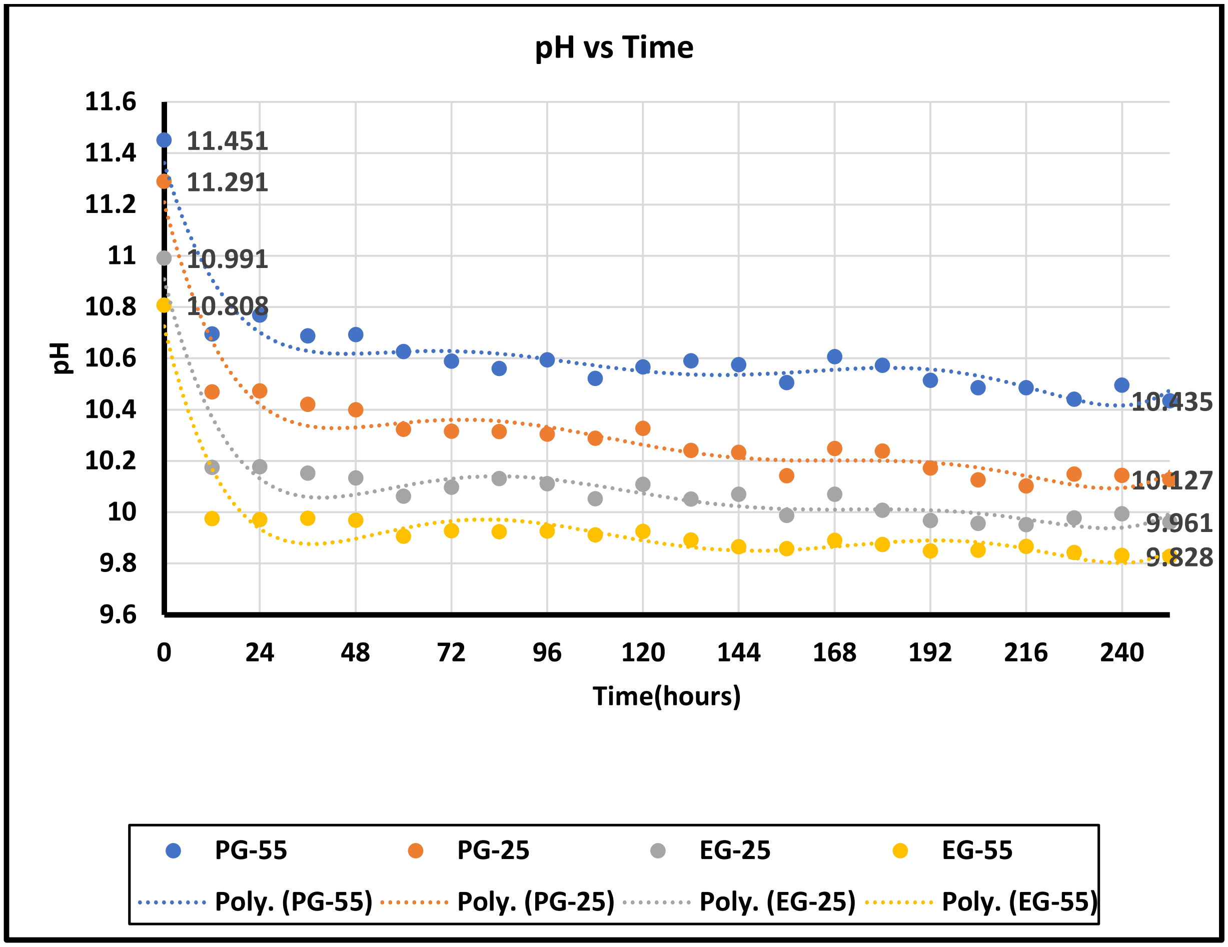

Graph 4.3.1.2: Variation – I Set – II pH vs Time

Set – I (EC)

The conductivity of the liquids seems to be increased in the case of jars that were kept unexposed. They all have an almost similar trend. EG-55 has a change of 47.55% which is the highest While PG-55 has a change of 13.6% which is the least among the four liquids. From the below graph we can say that the concentration of charge carriers increases in the liquids when kept unexposed to the outside air.

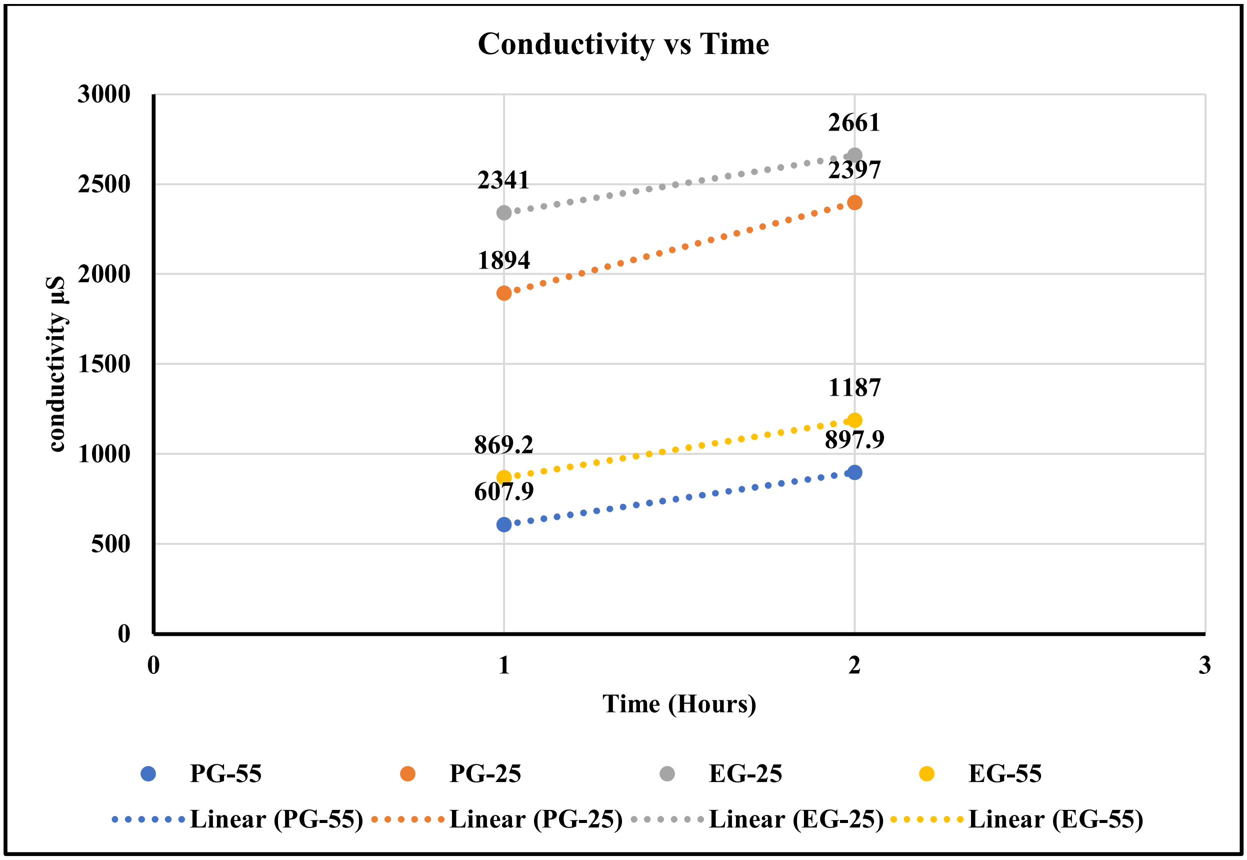

Graph 4.3.2.1: Variation – I Set – I Electrical conductivity vs Time

Set – II (EC)

In the second set of jars which were exposed to the outside air for a period approximately 1-2% of the time, the readings were taken twice every day with 12 hours gap. From the below graph it is observed that three of the liquids have a similar trend in conductivity level, but the conductivity value of PG-55 has constantly decreased with time. EG-55 has a change of 42.77% which is the highest While PG-55 has a change of 24.51% which is the least among the four liquids.[35]

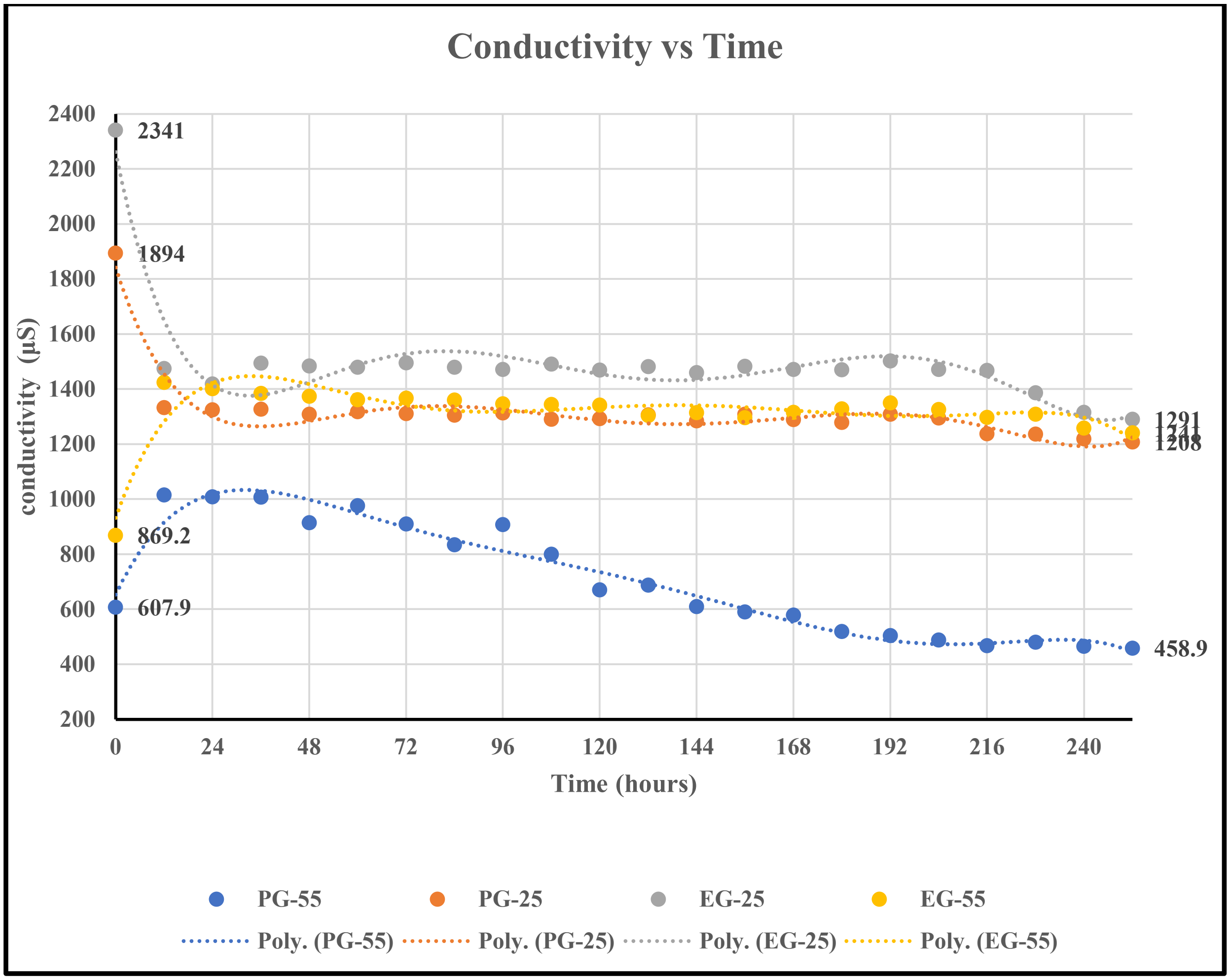

Graph 4.3.2.2: Variation – I Set – II Electrical conductivity vs Time

Set – I (ORP)

The ORP values in all the liquids which were kept un-exposed were reduced over time. From the below graph we can say that all the liquids are having fewer oxygen levels compared with the values at the start of the experiment. PG-55 has the highest change whereas EG-25 has the least change among the four liquids.[36]

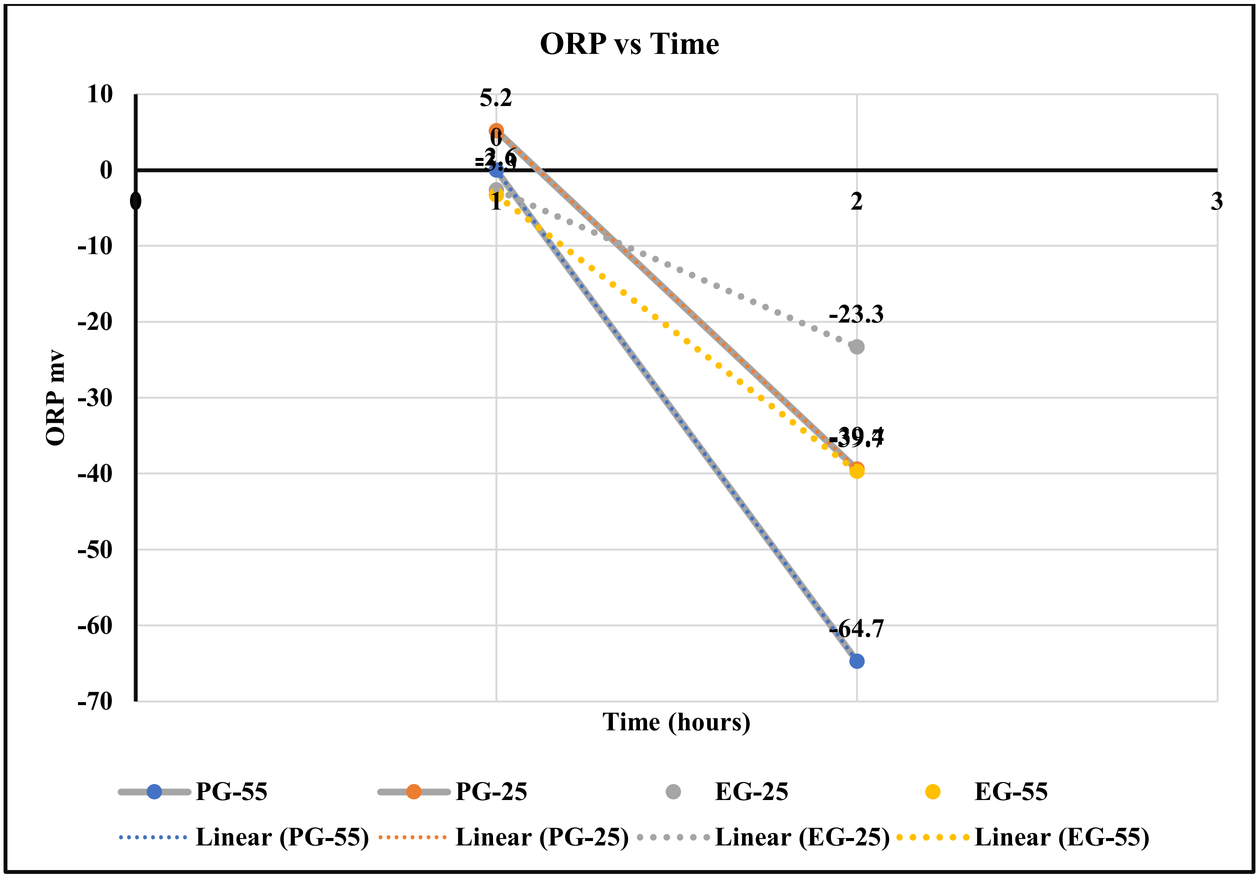

Graph 4.3.3.1: Variation – I Set – I ORP vs Time

Set- II (ORP)

From the below-plotted graph, we can state that ORP values were increased for all the liquids at the starting 24-hour period and then the ORP value kept on increasing. All the liquids seem to have a similar trend. PG-55 has the highest increase in ORP value whereas EG-25 has the least increase in ORP value.

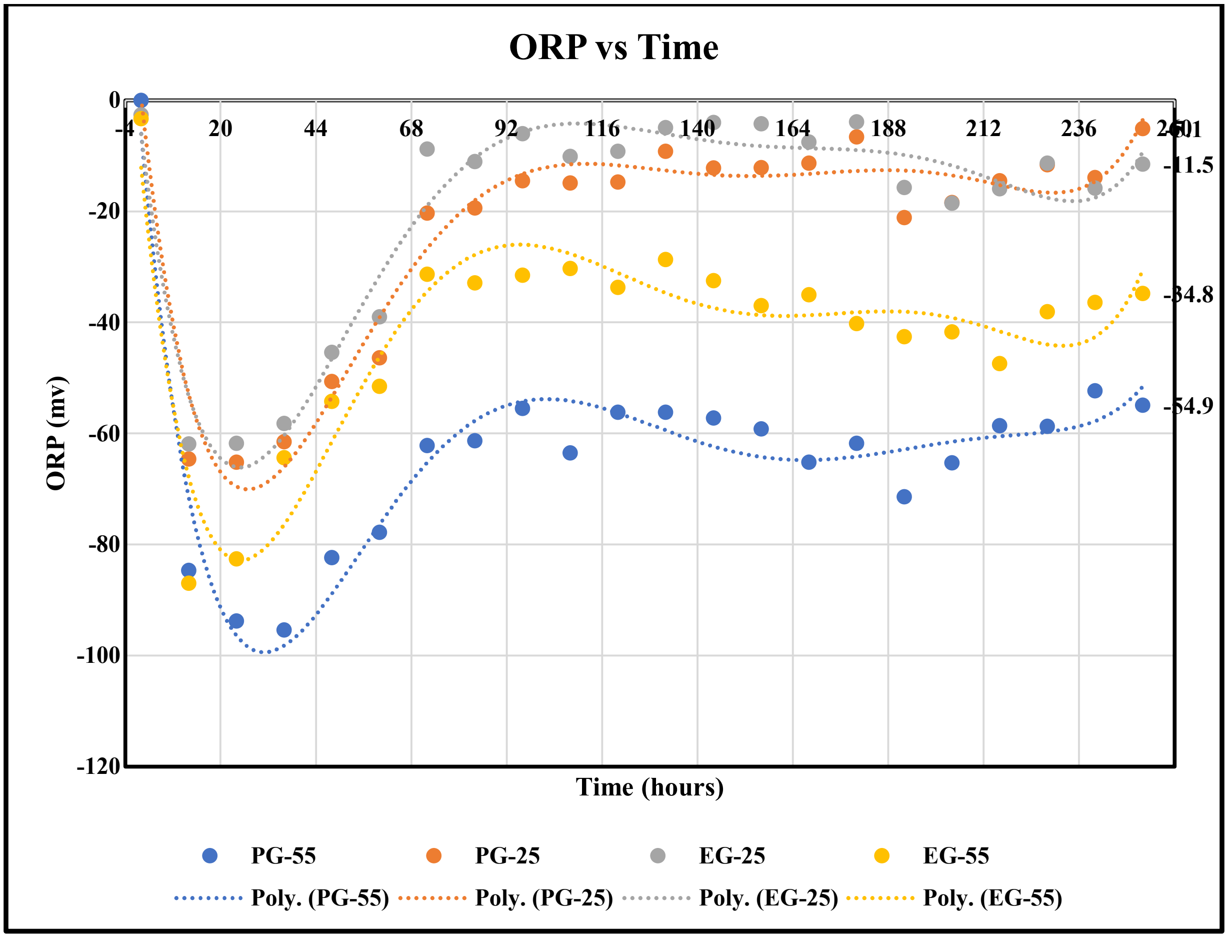

Graph 4.3.3.2: Variation – I Set – II ORP vs Time

Experiment – II

Variation – 2

Set – I (pH)

The pH values of all the liquids are measured initially and compared to the pH value at the end of the experiment. The end pH values of these liquids when the combination of materials is kept immersed in them is less than the pH values observed in Variation – I. The set-1 jar is unexposed to outside air during the whole test. From the below graph we can say that all the liquids have a similar trend in pH levels. EG-55 has a 3.9% change which is the least while EG-25 has a 5.07% change as the highest change in pH value among the four liquids.

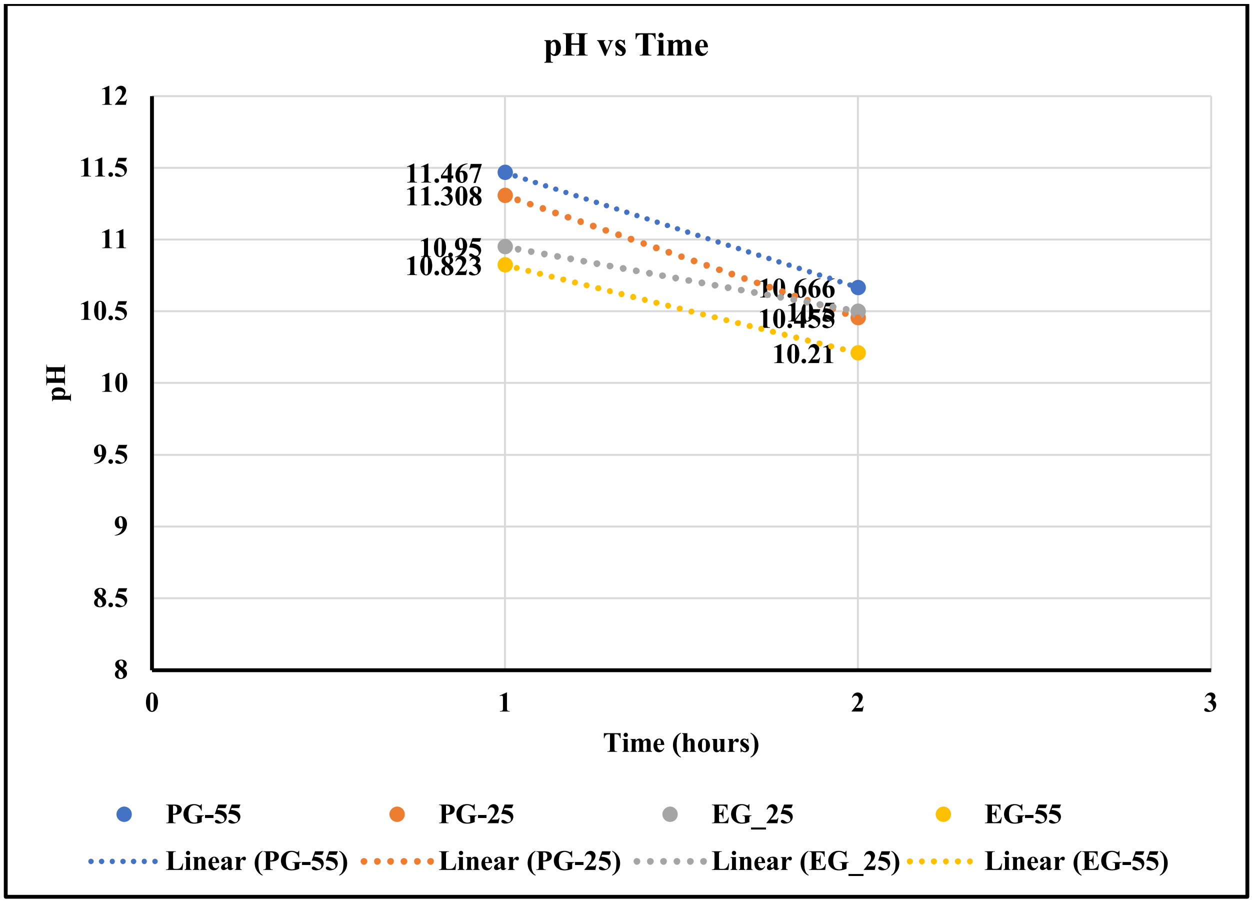

Graph 4.4.1.1: Variation – II Set – I pH vs Time

Set – II (pH)

In the second set of jars where the combination of materials are kept immersed were exposed to the outside air for a period of approximately 1-2% of the time, the readings were taken twice every day with 12 hours gap. From the below graph it is observed that all the liquids have a similar trend in pH levels even with periodic exposure to the outside air. EG-55 has the highest reduction of 14.42% EG- 25 has a reduction of 10.46% among the four liquids.[37]

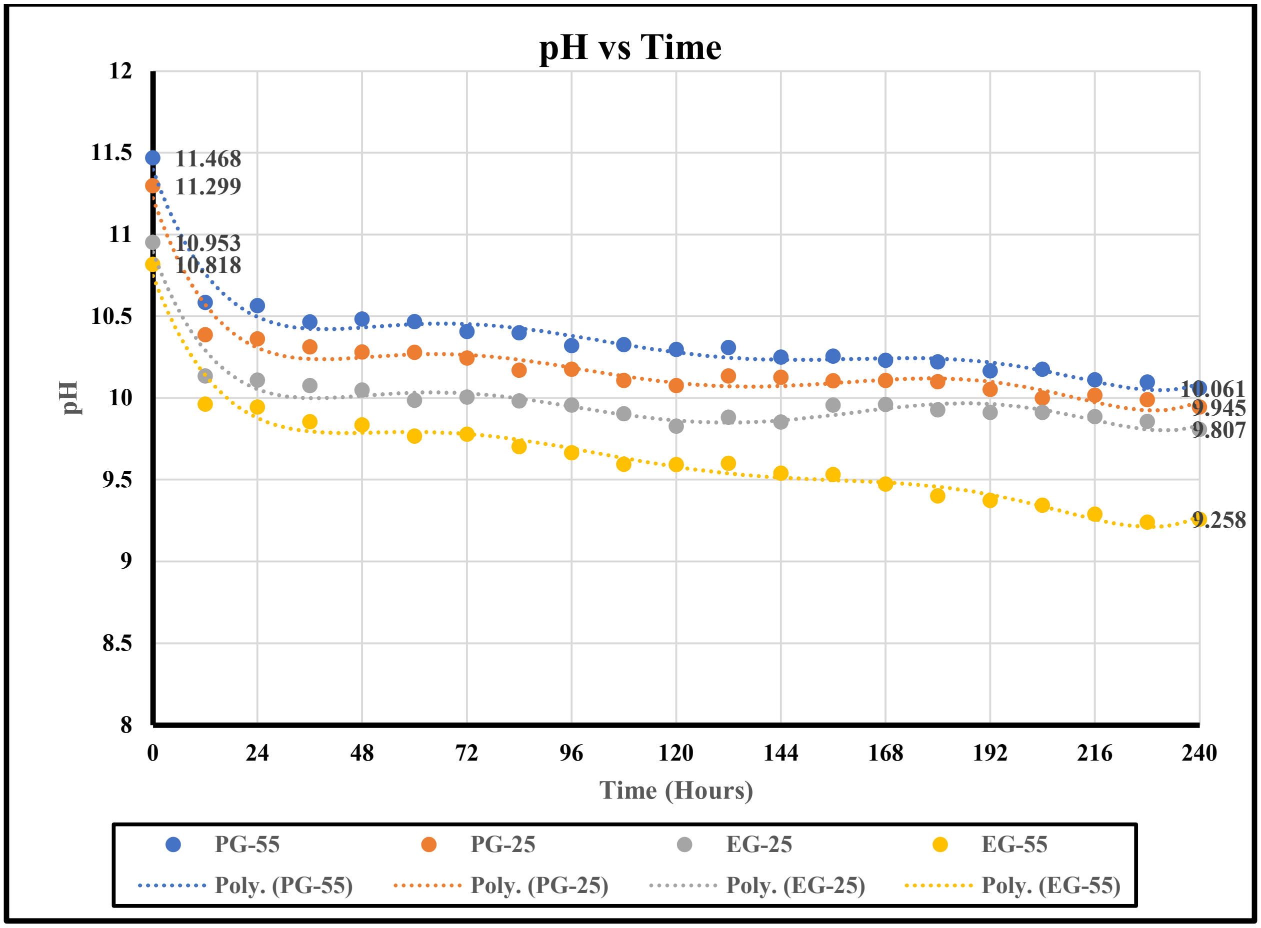

Graph 4.4.1.2: Variation – II Set – II pH vs Time

Set – I (conductivity)

The conductivity of the liquids seems to be increased in the case of jars with a combination of materials kept immersed. They all have an almost similar trend. PG-55 has a change of 30.78% which is the highest While EG-25 has a change of 7.97% which is the least among the four liquids. From the below graph we can say that the concentration of charge carriers increases in the liquids when kept unexposed to the outside air.

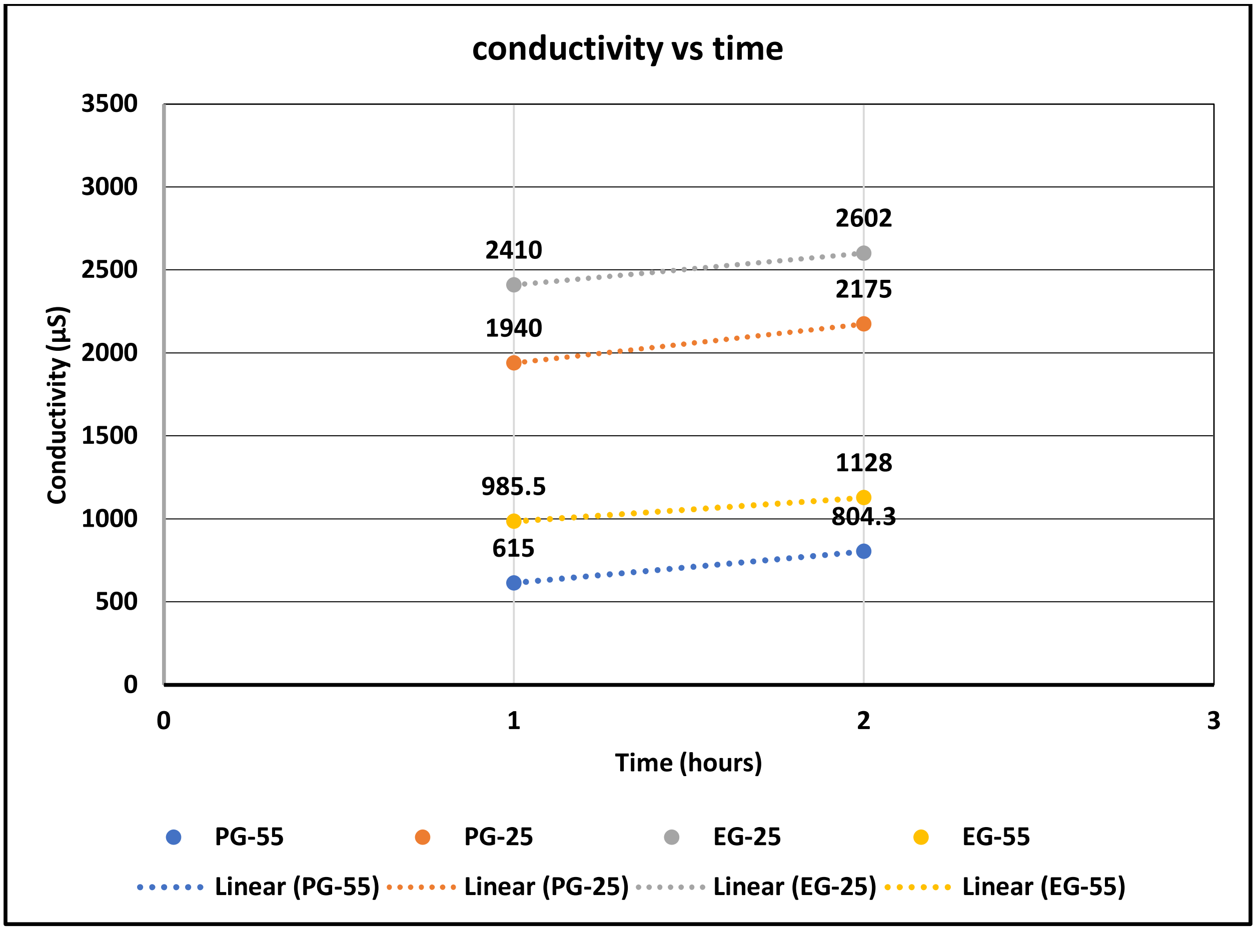

Graph 4.4.2.1: Variation – II Set – I Electrical conductivity vs Time

Set – II (conductivity)

In the second set of jars which were exposed to the outside air for a period approximately 1-2% of the time, From the below graph it is observed that all the liquids have a similar trend in conductivity level. All the liquids had almost similar charge concentrations throughout the experiment PG-55 has a change of 53.03% which is the highest While EG-55 has a change of 19.73% which is the least among the four liquids.[38]

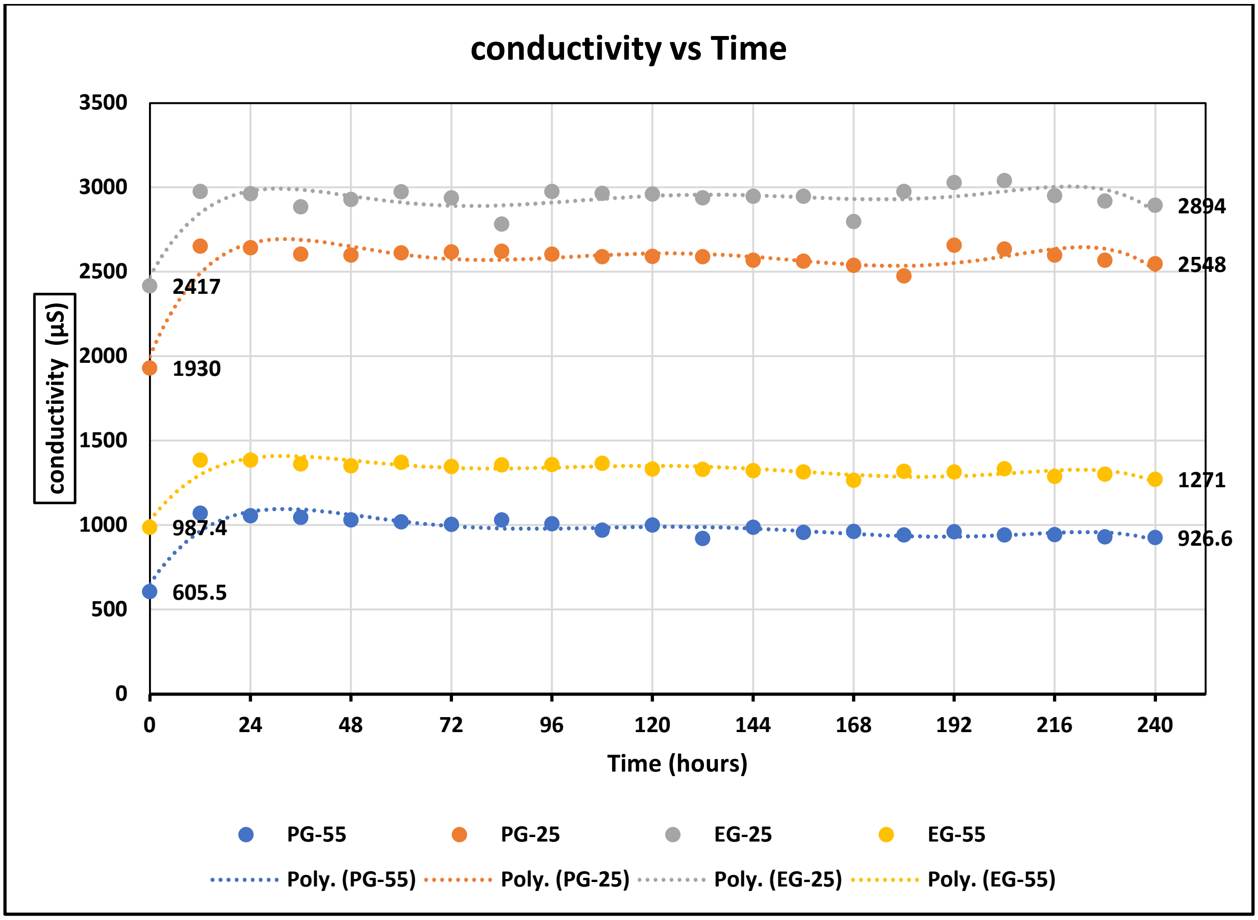

Graph 4.4.2.2: Variation – II Set – II Electrical conductivity vs Time

Set – II (ORP)

The ORP values in all the liquids when a combination of materials was kept immersed and kept un-exposed were reduced over time. From the below graph we can say that all the liquids are having fewer oxygen levels compared with the values at the start of the experiment. EG-55 has the least value and PG-25 has the highest value at the end of the experiment among the four liquids.

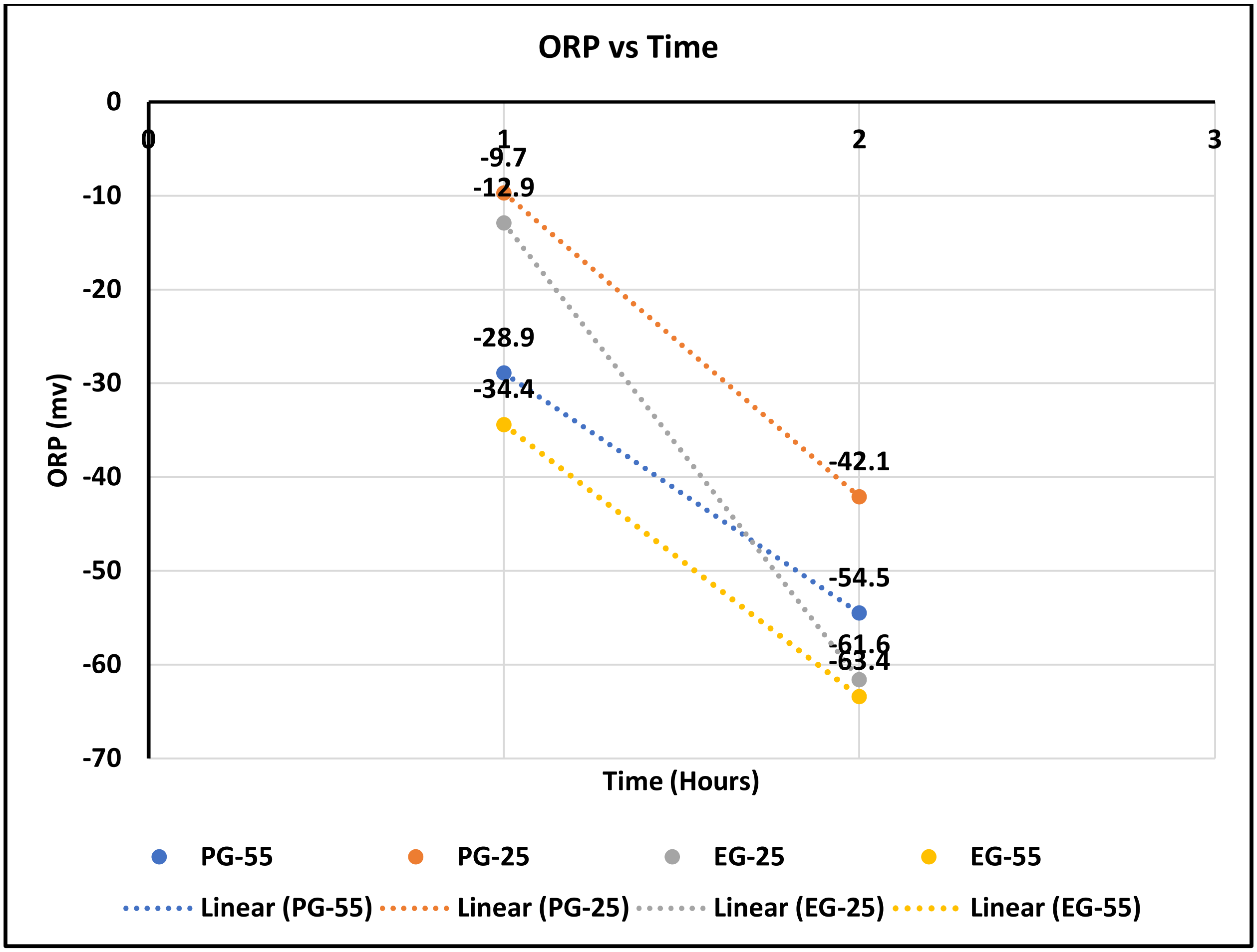

Graph 4.4.3.1: Variation – II Set – I ORP vs Time

Set – II (ORP)

From the below-plotted graph, we can state that ORP values were decreased for three of the liquids at the starting 24-hour period and then the ORP value kept on increasing. In the case of PG-25 ORP value never decreased but kept on increasing unevenly. All the liquids seem to have a similar trend after 24 hour period. PG-55 has the highest increase in ORP value whereas EG-25 has the least increase in ORP value among the four liquids.[39]

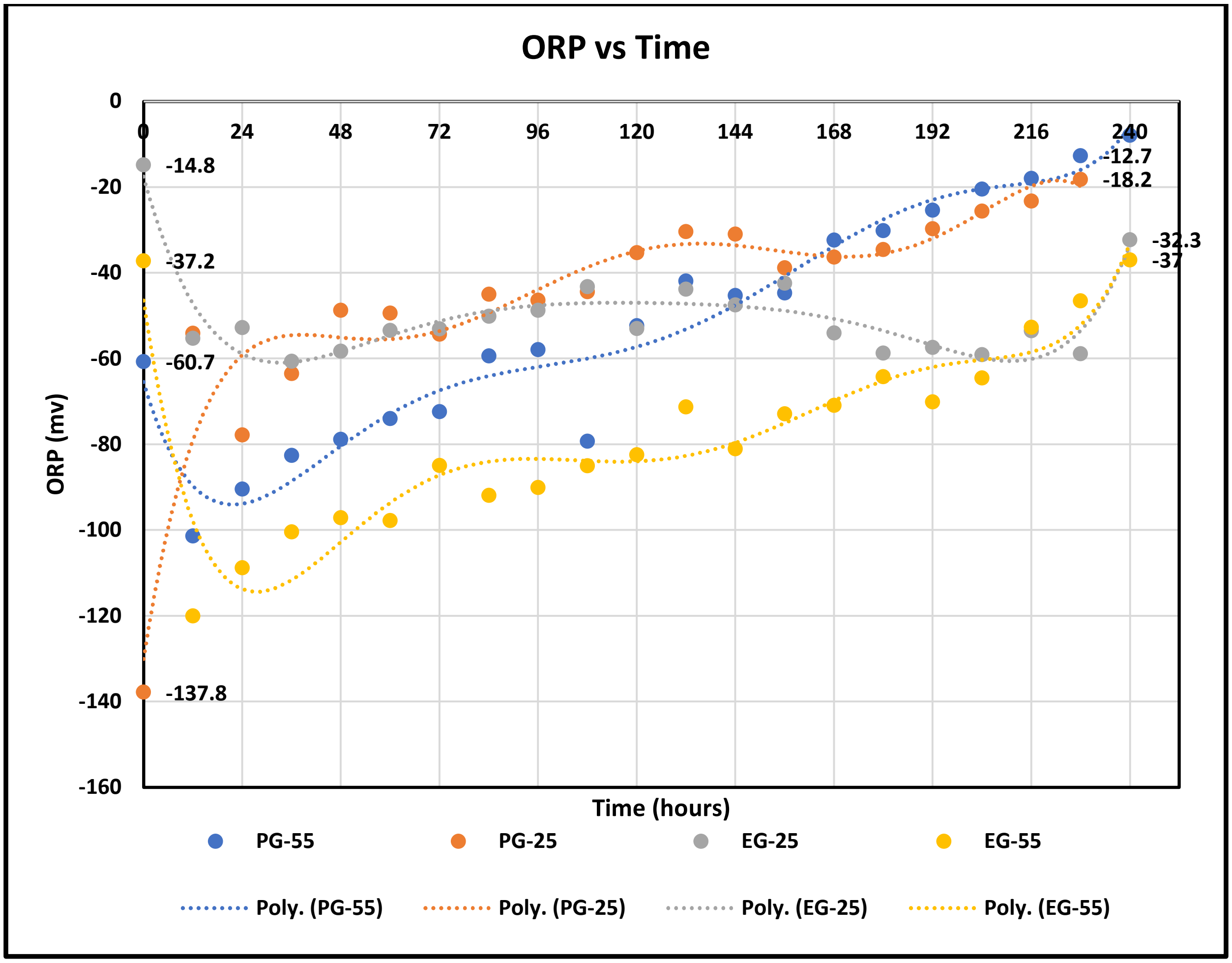

Graph 4.4.3.2: Variation – II Set – II ORP vs Time

Conclusion

From the experimental results, it can be said that corrosion is taking place inside the loop even after the addition of charge carriers or corrosion inhibitors.

The exposure of outside air is directly proportional to the rate of corrosion as the coolant liquids had a higher change in pH, Electrical conductivity, and ORP values than compared to that of jars that were kept un-exposed to the outside air.

The temperature of the coolant at the inlet should be kept at lower limits which can reduce the corrosion rate. This may increase the cooling power for a data center facility, but it can save many other costs such as pumping power maintenance costs and repair costs.

When a cold plate is replaced due to blockage by corrosion the whole server might be shut down for its repair which can cost an ample amount.

The addition of charge carriers should be done to the liquid coolants at regular periods to keep the corrosion level minimum and to increase the life of cold plates.

Future Work

Investigate the trend of the variation in coolant properties for the coolants at two more concentrations PG-25 and EG-55 to compare the effects of concentrations of the coolants that are used in the data center cooling industry

To find the corrosion level by studying the surface topography of the cold plate microchannels using SEM.

Studying the surface topography of the materials which were kept immersed in the coolant liquids and comparing the corrosion levels in between them.

References

[1] G. Kini et al., "Corrosion in Liquid Cooling Systems with Water-Based Coolant – Part 1: Flow Loop Design for Reliability Tests," 2020 19th IEEE Intersociety Conference on Thermal and Thermomechanical Phenomena in Electronic Systems (ITherm), 2020, pp. 422-428, doi: 10.1109/ITherm45881.2020.9190607.

[2] C. -U. Kim et al., "Corrosion in Liquid Cooling Systems with Water-Based Coolant – Part 2: Corrosion Reliability Testing and Failure Model," 2020 19th IEEE Intersociety Conference on Thermal and Thermomechanical Phenomena in Electronic Systems (ITherm), 2020, pp. 429-434, doi: 10.1109/ITherm45881.2020.9190565.

[3] https://datacenterfrontier.com/google-shifts-to-liquid-cooling-for-ai-data-crunching/

[4] https://www.ddcoatings.co.uk/2276/what-is-pitting-corrosion

[5]https://www.solaracks.com/what-is-galvanic-corrosionbimetallic-corrosiondissimilar-metal-corrosion/

[6] https://www.researchgate.net/post/ORP_in_Boiler_and_Steam_sample

[7] https://sensorex.com/technical-education/

[8] https://www.watlow.com/products/heaters/specialty-heaters/ultramic-ceramic-heaters

[9] https://www.amazon.com/bayite-BYT-7A015-Heater-Circulation-Adapter/dp/B01G305PK0

[10] https://www.keyence.com/products/process/pressure/gp-m/models/gp-m010/

[11] https://www.mcmaster.com/4742K13/

[12] https://www.masterflex.com/i/masterflex-in-line-strainer-mesh-304-stainless-steel-low-profile-15-micron/2959541

[13] https://www.polyscience.com/products/chillers/6000-series/centrifugal-pump

[14] https://www.kelvion.com/products/product/gwh-series/

[15] https://www.hannainst.com/hi5522-research-grade-ph-orp-ise-and-ec-tds-salinity-resistivity-meter-with-cal-check.html

[16] https://www.hannainst.com/hi1131b-refillable-combination-ph-electrode.html

[17] https://www.hannainst.com/four-ring-ec-tds-probe-with-internal-temperature-sensor-hi76312.html

[18] https://www.hannainst.com/hi3131b-refillable-combination-orp-electrode.html

[19] https://www.amazon.com/dp/B07KRQVWJR/ref=cm_sw_r_apan_glt_fabc_1YGTJA0XTW3K4F2K9S60

[20] https://www.fluke.com/en-us/product/calibration-tools/temperature-calibrators/fluke-calibration-6109a-7109a

[21] Shah, J.M., Anand, R., Saini, S., Cyriac, R., Agonafer, D., Singh, P., & Kaler, M., 2019, "Development of a Technique to Measure Deliquescent Relative Humidity of Particulate Contaminants and Determination of the Operating Relative Humidity of a Data Center, " Proceedings of the ASME 2019 International Technical Conference and Exhibition on Packaging and Integration of Electronic and Photonic Microsystems. ASME 2019 International Technical Conference and Exhibition on Packaging and Integration of Electronic and Photonic Microsystems. Anaheim, California, USA. October 7–9, 2019. V001T02A016. ASME. https://doi.org/10.1115/IPACK2019-6601

[22] Saini, Satyam, 2018, "Airflow Path and Flow Pattern Analysis of Sub-Micron Particulate Contaminants in a Data Center with Hot Aisle Containment System Utilizing Direct Air Cooling," The University of Texas at Arlington, Arlington, TX.

[23] Saini, S., Shahi, P., Bansode, P., Siddarth, A., Agonafer, D., 2020, "CFD Investigation of Dispersion of Airborne Particulate Contaminants in a Raised Floor Data Center," 36th Semiconductor Thermal Measurement, Modeling & Management Symposium (SEMI-THERM), San Jose, CA, USA, 2020, pp. 39-47, doi: 10.23919/SEMITHERM50369.2020.9142865.

[24] Thirunavakkarasu, G., Saini, S., Shah, J.M., Agonafer, D., 2018, "Air Flow Pattern and Path Flow Simulation of Airborne Particulate Contaminants in a High-Density Data Center Utilizing Airside Economization," Proceedings of the ASME 2018 International Technical Conference and Exhibition on Packaging and Integration of Electronic and Photonic Microsystems. ASME 2018 International Technical Conference and Exhibition on Packaging and Integration of Electronic and Photonic Microsystems. San Francisco, California, USA. August 27–30, 2018. V001T02A011. ASME. https://doi.org/10.1115/IPACK2018-8436

[25] Saini, S., Adsul, K.K., Shahi, P., Niazmand, A., Bansode, P., & Agonafer, D., 2020, "CFD Modeling of the Distribution of Airborne Particulate Contaminants Inside Data Center Hardware," Proceedings of the ASME 2020 International Technical Conference and Exhibition on Packaging and Integration of Electronic and Photonic Microsystems. ASME 2020 International Technical Conference and Exhibition on Packaging and Integration of Electronic and Photonic Microsystems. Virtual, Online. October 27–29, 2020. V001T08A005. ASME. https://doi.org/10.1115/IPACK2020-2590

[26] Gandhi, D., Chowdhury, U., Chauhan, T., Bansode, P.V., Saini., S, Shah, J.M., & Agonafer, D., 2019, "Computational Analysis for Thermal Optimization of Server for Single Phase Immersion Cooling," Proceedings of the ASME 2019 International Technical Conference and Exhibition on Packaging and Integration of Electronic and Photonic Microsystems. ASME 2019 International Technical Conference and Exhibition on Packaging and Integration of Electronic and Photonic Microsystems. Anaheim, California, USA. October 7–9, 2019. V001T02A013. ASME. https://doi.org/10.1115/IPACK2019-6587

[27] Shinde, P.A., Bansode, P.V., Saini, S., Kasukurthy, R., Chauhan, T., Shah, J.M., & Agonafer, D., 2019, "Experimental Analysis for Optimization of Thermal Performance of a Server in Single

Phase Immersion Cooling," Proceedings of the ASME 2019 International Technical Conference and Exhibition on Packaging and Integration of Electronic and Photonic Microsystems. ASME 2019 International Technical Conference and Exhibition on Packaging and Integration of Electronic and Photonic Microsystems. Anaheim, California, USA. October 7–9, 2019. V001T02A014. ASME. https://doi.org/10.1115/IPACK2019-6590

[28] Niazmand, A., Murthy, P., Saini, S., Shahi, P., Bansode, P., & Agonafer, D., 2020, "Numerical Analysis of Oil Immersion Cooling of a Server Using Mineral Oil and Al2O3 Nanofluid," Proceedings of the ASME 2020 International Technical Conference and Exhibition on Packaging and Integration of Electronic and Photonic Microsystems. ASME 2020 International Technical Conference and Exhibition on Packaging and Integration of Electronic and Photonic Microsystems. Virtual, Online. October 27–29, 2020. V001T08A009. ASME. https://doi.org/10.1115/IPACK2020-2662

[29] Kumar, A., Shahi, P., Saha, S.K., 2018, "Experimental study of latent heat thermal energy storage system for medium temperature solar applications," In Proceedings of the 4th World Congress on Mechanical, Chemical, and Material Engineering (MCM'18), Madrid, Spain, pp. 16-18

[30] Shahi, P., Agarwal, S., Saini, S., Niazmand, A., Bansode, P., & Agonafer, D., 2020, "CFD Analysis on Liquid Cooled Cold Plate Using Copper Nanoparticles," Proceedings of the ASME 2020 International Technical Conference and Exhibition on Packaging and Integration of Electronic and Photonic Microsystems. ASME 2020 International Technical Conference and Exhibition on Packaging and Integration of Electronic and Photonic Microsystems. Virtual, Online. October 27–29,2020.V001T08A007. ASME. https://doi.org/10.1115/IPACK2020-2592

[31] Niazmand, A., Chauhan, T., Saini, S., Shahi, P., Bansode, P.V., & Agonafer, D., 2020, "CFD Simulation of Two-Phase Immersion Cooling Using FC-72 Dielectric Fluid." Proceedings of the ASME 2020 International Technical Conference and Exhibition on Packaging and Integration of Electronic and Photonic Microsystems. ASME 2020 International Technical Conference and Exhibition on Packaging and Integration of Electronic and Photonic Microsystems. Virtual, Online. October 27–29, 2020. V001T07A009. ASME. https://doi.org/10.1115/IPACK2020-2595

[32] Shah, JM, Bhatt, C, Rachamreddy, P, Dandamudi, R, Saini, S, & Agonafer, D. "Computational Form Factor Study of a 3rd Generation Open Compute Server for Single-Phase Immersion Cooling." Proceedings of the ASME 2019 International Technical Conference and Exhibition on Packaging and Integration of Electronic and Photonic Microsystems. ASME 2019 International Technical Conference and Exhibition on Packaging and Integration of Electronic and Photonic Microsystems. Anaheim, California, USA. October 7–9, 2019. V001T02A017. ASME. https://doi.org/10.1115/IPACK2019-6602

[33] Shahi, P., Saini, S., Bansode, P., and Agonafer, D., 2021, "A Comparative Study of Energy Savings in a Liquid-Cooled Server by Dynamic Control of Coolant Flow Rate at Server Level," in IEEE Transactions on Components, Packaging and Manufacturing Technology, 11(4), pp. 616-624, doi: 10.1109/TCPMT.2021.3067045

[34] Shah, J. M., Anand, R., Singh, P., Saini, S., Cyriac, R., Agonafer, D., and Kaler, M. (June 23, 2020). "Development of a Precise and Cost-Effective Technique to Measure Deliquescent Relative Humidity of Particulate Contaminants and Determination of the Operating Relative Humidity of a Data Center Utilizing Airside Economization." ASME. J. Electron. Packag. December 2020; 142(4): 041103. https://doi.org/10.1115/1.4047469

[35] Saini, S., Shah, J. M., Shahi, P., Bansode, P., Agonafer, D., Singh, P., Schmidt, R., and Kaler, M. (September 15, 2021). "Effects of Gaseous and Particulate Contaminants on Information Technology Equipment Reliability—A Review." ASME. *J. Electron. Packag*. September 2022; 144(3): 030801. https://doi.org/10.1115/1.4051255

[36] Shah, J. M., Padmanaban, K., Singh, H., Duraisamy Asokan, S., Saini, S., and Agonafer, D. (October 14, 2021). "Evaluating the Reliability of Passive Server Components for Single-Phase Immersion Cooling." ASME. *J. Electron. Packag*. June 2022; 144(2): 021109. https://doi.org/10.1115/1.4052536

[37] Shahi, P., Deshmukh, A. P., Hurnekar, H. Y., Saini, S., Bansode, P., Kasukurthy, R., and Agonafer, D. (November 22, 2021). "Design, Development, and Characterization of a Flow Control Device for Dynamic Cooling of Liquid-Cooled Servers." ASME. *J. Electron. Packag*. December 2022; 144(4): 041008. https://doi.org/10.1115/1.4052324

[38] Chowdhury, U, Sahini, M, Siddarth, A, Agonafer, D, & Branton, S. "Characterization of an Isolated Hybrid Cooled Server With Failure Scenarios Using Warm Water Cooling." *Proceedings of the ASME 2017 International Technical Conference and Exhibition on Packaging and Integration of Electronic and Photonic Microsystems collocated with the ASME 2017 Conference on Information Storage and Processing Systems*. *ASME 2017 International Technical Conference and Exhibition on Packaging and Integration of Electronic and Photonic Microsystems*. San Francisco, California, USA. August 29–September 1, 2017. V001T02A002. ASME. https://doi.org/10.1115/IPACK2017-74028

[39] Chowdhury, U, Hendrix, W, Craft, T, James, W, Sutaria, A, & Agonafer, D. "Optimal Design and Modeling of Server Cabinets With In-Row Coolers and Air Conditioning Units in a Modular Data Center." *Proceedings of the ASME 2019 International Technical Conference and Exhibition*

on Packaging and Integration of Electronic and Photonic Microsystems. *ASME 2019 International Technical Conference and Exhibition on Packaging and Integration of Electronic and Photonic Microsystems*. Anaheim, California, USA. October 7–9, 2019. V001T02A009. ASME. https://doi.org/10.1115/IPACK2019-6522

Biological Information

Lochan sai Reddy Chinthaparthy was born in India. He received his Bachelor of Engineering degree in Mechanical Engineering from Vignan Institute of Technology and Science, Deshmukh Village, Nalgonda District, Telangana state, India in June 2019. He started his Master's studies in Mechanical Engineering at the University of Texas at Arlington in Spring 2020. He received his Master of Science in Mechanical Engineering from The University of Texas at Arlington, in December 2021. His interests include reliability in the data center, thermal performance of cold plates, Reliability of coolant liquids, Analysis of heat exchangers etc.